CIVλ1549 as an Eigenvector 1 Parameter for Active Galactic Nuclei

Jack W. Sulentic[1], Rumen Bachev[1], Paola Marziani[2],
C. Alenka Negrete[3], Deborah Dultzin[3]

ABSTRACT

We have been exploring a spectroscopic unification for all known types of broad line emitting AGN. The 4D Eigenvector 1 (4DE1) parameter space shows promise as a unification capable of organizing quasar diversity on a sequence primarily governed by Eddington ratio. This paper considers the role of CIVλ1549 measures with special emphasis on the CIVλ1549 line shift as a principal 4DE1 diagnostic. We use HST archival spectra for 130 sources with S/N high enough to permit reliable CIVλ1549 broad component measures. We find a CIV$\lambda1549_{\rm BC}$ profile blueshift that is strongly concentrated among (largely radio-quiet: RQ) sources with FWHM(H$\beta_{\rm BC}$) $\lesssim 4000$ km s^{-1} (which we call Population A). Narrow line Seyfert 1 (NLSy1, with FWHM H$\beta \leq 2000$ km s^{-1}) sources belong to this population but do not emerge as a distinct class. The systematic blueshift, widely interpreted as arising in a disk wind/outflow, is not observed in broader line AGN (including most radio-loud (RL) sources but also ~ 25 % of RQ) which we call Population B. We find new correlations between FWHM(CIV$\lambda1549_{\rm BC}$) and CIVλ1549 line shift as well as the equivalent width of CIVλ1549. They are seen only in Pop. A sources. Broader-lined sources show random scatter. CIVλ1549 measures enhance the apparent dichotomy between sources with FWHM(H$\beta_{\rm BC}$) *less and greater than* 4000 km s^{-1} (Sulentic et al. 2000a) suggesting that it has more significance in the context of Broad Line Region structure than the more commonly discussed RL vs. RQ dichotomy. Black hole masses computed from

[1]Department of Physics and Astronomy, University of Alabama, Tuscaloosa, AL 35487, USA; giacomo@merlot.astr.ua.edu

[2]INAF, Osservatorio Astronomico di Padova, Vicolo dell'Osservatorio 5, I-35122 Padova, Italy; paola.marziani@oapd.inaf.it

[3]Instituto de Astronomía, Universidad Nacional Autonoma de México (UNAM), Apdo. Postal 70-264, 04510 Mexico D.F., Mexico; deborah@astroscu.unam.mx

FWHM CIVλ1549$_{\rm BC}$ for about 80 AGN indicate that the CIVλ1549 width is a poor virial estimator. Comparison of mass estimates derived from H$\beta_{\rm BC}$ and CIVλ1549 reveals that the latter show different and nonlinear offsets for population A and B sources. A significant number of sources also show narrow line CIVλ1549 emission that must be removed before CIVλ1549$_{\rm BC}$ measures can be made and interpreted effectively. We present a recipe for CIVλ1549 narrow component extraction.

Subject headings: quasars: general, emission lines; line: profiles

1. Introduction

The search for a parameter space that might provide spectroscopic unification for all classes of broad line emitting AGN motivated the "4D Eigenvector 1" (4DE1) concept (Sulentic et al. 2000a,b). Such a correlation space might serve as an equivalent to the stellar H-R Diagram. Domain space occupation differences and parameter correlations might then provide the empirical clues from which underlying physics could be inferred. At the very least it can be used to highlight important differences between sources that can also drive our physical understanding of the geometry, kinematics and physics of the broad line emitting region (BLR). From the outset it was expected that a parameter space for AGN would require more than two dimensions because source orientation and "physics" (e.g., black hole mass $M_{\rm BH}$ and Eddington ratio) drive AGN parameter values and correlations. A suitably chosen n-dimensional space should help to remove the degeneracy between these two drivers.

4DE1 has roots in the PCA analysis of the Bright Quasar Sample (87 sources; Boroson & Green 1992) as well as in correlations that emerged from ROSAT (e.g. Wang et al. 1996). 4DE1 as we define it involves BG92 measures: (1) full width half maximum of broad Hβ (FWHM Hβ) and (2) equivalent width ratio of optical FeII and broad Hβ: $R_{\rm FeII}$= W(FeII λ4570)/W(H$\beta_{\rm BC}$). We added a Wang et al. (1996)-defined measure involving (3) the soft X-ray photon index ($\Gamma_{\rm soft}$) and a measure of (4) CIVλ1549 broad line profile velocity displacement at half maximum ($c(\frac{1}{2})$) to arrive at our 4DE1 space. Other points of departure from BG92 involve our comparison of RQ and RL sources as well as subordination of BG92 [OIII]λ5007 measures (although see Zamanov et al. 2002; Marziani et al. 2003a). Finally we divide sources into two AGN populations using a simple division at FWHM H$\beta_{\rm BC}$ =4000 km s^{-1} with sources narrower and broader than this value designated Pop. A and B respectively. It was motivated by the observation that almost all RL sources show FWHMH$\beta_{\rm BC} \gtrsim$ 4000 km s^{-1} (Sulentic et al. 2000b). This division appears to be more effective than the more traditional divisions into: (1) RQ-RL sources as well as (2) NLSy1 sources defined with

FWHM(H$\beta_{\rm BC}$)$\lesssim$ 2000 km s^{-1} and broader line sources above this value. Results presented in this paper strongly support the Pop. A-B distinction. Exploration of possible physical drivers of source occupation/correlation in 4DE1 (Marziani et al. 2001, 2003b; Boroson 2002) suggest that it is primarily driven by the luminosity to black hole mass ($M_{\rm BH}$) ratio which is proportional to the Eddington ratio ($L_{\rm bol}/L_{\rm Edd}$) with Pop. A sources being high accreting/low $M_{\rm BH}$ AGN, while Pop. B being low accreting/large $M_{\rm BH}$ AGN.

Past 4DE1 studies focused on the optical 4DE1 plane (FWHM Hβ vs. $R_{\rm FeII}$) at low redshift because more high S/N optical spectra exist than UV or X-ray measures. Complementary high-z measures of the Hβ region at IR wavelengths are ongoing (Sulentic et al. 2004, 2006a). This paper focuses on an expanded sample of CIVλ1549 measures and explores their utility as 4DE1 parameters. The work is supplemental to a recent paper (Bachev et al. 2004) that discusses data processing and analysis of 123 CIVλ1549 spectra from the HST archive. The new CIVλ1549 sample is almost twice the size of the one discussed in the defining 4DE1 paper (Sulentic et al. 2000a). We present (§2) new 4DE1 correlation diagrams involving measures of the CIVλ1549 line shift and then look (§2.3) at the implications of CIVλ1549-defined source occupation for BLR structure and for the hypothesized AGN Populations (A and B; §3). Section 4 discusses the reality of a significant narrow line CIVλ1549 component in many sources and compares our CIVλ1549 measures with other recent studies utilizing the same spectra. Section 5 considers the implications of our CIVλ1549 results on the use of FWHM CIVλ1549 to estimate black holes masses.

2. CIVλ1549 Line Measures and Correlations

2.1. Sample Definition and Data Analysis

We searched the HST archive[1] and found useable CIVλ1549 spectra for 130 out 141 low-redshift sources. Excluded sources are mostly CIVλ1549 BAL quasars where reliable measures of the CIVλ1549 emission profile are difficult. OI 363 was not included because of low S/N. IRAS 13218+0552 (J132419.9+053705) was excluded because it shows no broad lines that would warrant a Type 1 AGN designation. We assume that our sample is large enough to reasonably represent the broad emission line properties of low z AGN. It is likely to be the only UV dataset of reasonable quality quasar spectra in the foreseeable future. The sample should be particularly valuable for RQ vs. RL comparisons because the two popula-

[1]Datasets covering the CIVλ1549 sources listed in Table 1 can be all identified and retrieved from the WWW site at URL `http://archive.stsci.edu/hst` and are not reported here. A list with the actual datasets employed is available from the authors at URL `http://web.oapd.inaf.it/marziani`.

tions are almost equally represented while in a complete sample only ≈ 10 % are found to be RL (Jiang et al. 2006; Cirasuolo et al. 2003; Sulentic et al. 2003). A PG quasar subsample was identified and includes 43 sources with 26% RL reflecting the overrepresentation of RL sources in the HST archive.

The uncertainty due to instrumental errors in wavelength calibration are estimated to be ≈ 200 km s^{-1} (Marziani et al. 1996). In order to reduce wavelength calibration errors HST spectra were "re-aligned" using expected rest-wavelengths of strong low-ionization, Galactic absorption-lines including Mg II λ2796.35, Mg II λ2803.53, Fe II λ2600.17, Fe II λ2586.65, Fe II λ2382.77, Fe II λ2374.46, Fe II λ2344.21, Al II λ1670.79, Si II λ1526.71, C II λ1334.53, Si II λ1260.42 (Savage et al. 2000). In case only one or two Galactic lines were available in the spectra, any shift between expected Galactic line wavelength and the wavelength measured on the spectra was double checked to avoid spurious results due to low S/N. Suitable Galactic lines were found for 110 sources in our sample with three or more lines available for 71 sources. The average rms of the residuals between measured line wavelengths after re-alignment and tabulated wavelengths is $< rms >\approx$ 40 km s^{-1}. This provides an estimate of the wavelength calibration uncertainty (at 1σ confidence level) for the re-aligned spectra.

The broad component of CIVλ1549 (CIV$\lambda1549_{\rm BC}$) was extracted after correction for contaminating lines (NIV]λ1486, and especially HeIIλ1640and OIII]λ1663) and subtraction of Fe$\rm II_{UV}$ emission (details of data reduction are given in Bachev et al. (2004) and Marziani et al. (1996)). The continuum underlying CIVλ1549 was estimated from nearby regions that are free of strong emission lines (between the λ1400 blend and NIV]λ1486 on the blue side as well as 1700 – 1800 Å on the red side). A narrow component (CIV$\lambda1549_{\rm NC}$) was subtracted from the profile when warranted. There is still disagreement about the existence, frequency of occurrence and strength of any CIV$\lambda1549_{\rm NC}$. We discuss the evidence for NLR CIVλ1549 and describe our CIV$\lambda1549_{\rm NC}$ subtraction procedure in §4.

2.2. Immediate Results

Fig. 1 shows individual cleaned CIV$\lambda1549_{\rm BC}$ profiles fit with high-order spline functions to minimize effects of noise and to preserve the complexity of the shape (following Marziani et al. 1996, 2003a). The spline fit is shown as a thick line in Fig. 1 while identified narrow components (that were subtracted in this analysis) are seen above the spline.

Table 1 gives an identification list of all sources shown in Figure 1 along with 4DE1 optical and X-ray parameters. Table 1 includes: Column 1 – IAU code identification; Col.

2 - a common name for the source; Col. 3 – available source redshift with number of significant figures indicating accuracy of the determination; Col. 4 – redshift reference. Col. 5 – an asterisk indicates that the sources belongs to the Boroson & Green (1992) PG sample, a "B" indicates that the source is a "blue outlier" (Zamanov et al. 2002). Col. 6 – Galactic absorption ($A_{\rm B}$, in magnitudes), Col. 7 – available measures of FWHM for Hβ broad component (FWHM(H$\beta_{\rm BC}$), units km s^{-1}) taken from Marziani et al. (2003b), measures of SDSS spectra or, as a last resort, literature spectra; Col. 8 – measures of the ratio $R_{\rm FeII}$ from same sources as Col. 7; Col. 9 – decimal logarithm of the specific flux at 4400 Å over the flux at 6 cm. A source is assumed radio-loud if log $R_{\rm K}\geq$ 1.8; Col. 10 – a measure of the soft X-ray excess (photon index $\Gamma_{\rm soft}$), from (Sulentic et al. 2000a,b) and from various literature sources.

The reported optical redshifts come from measures of low-ionization optical emission lines (LILs), typically H$\beta_{\rm NC}$, H$\gamma_{\rm NC}$, and H$\alpha_{\rm NC}$ supplemented by values derived from [OIII]$\lambda\lambda$4959,5007 if the source is not a blue outlier (see Marziani et al. 2003a; Zamanov et al. 2002). In these cases, the agreement between LIL and high-ionization lines (HILs) is reasonable within the accuracy limits of the present study. We remind that "blue outliers" i.e., sources with large [OIII]$\lambda\lambda$4959,5007 blueshift relative to optical LILs, tend to be extreme Pop. A sources with very weak [OIII]$\lambda\lambda$4959,5007, and are relatively rare. The recipe described in Marziani et al. (2003a) is applied for all sources with references indicated as ESO, SPM, M03, M96, SDSS, G99. All other sources have redshift measured on the basis of the optical lines. None of the remaining sources are likely to be blue outliers on the basis of published spectra so redshift computed using optical lines should be a reliable estimate even if [OIII]$\lambda\lambda$4959,5007 lines were used.

Table 2 presents our CIVλ1549 parameter measures with format as follows: Column 1 – IAU code; Col. 2 – specific continuum flux at 1550Å (units erg s^{-1} Å^{-1} cm$^{-2}\times10^{14}$); Col. 3 – flux in the CIV$\lambda1549_{\rm NC}$ (units erg s^{-1} cm$^{-2}\times10^{13}$); Col. 4 – Peak CIV$\lambda1549_{\rm NC}$ radial velocity, in km s^{-1}; Col. 5 – flux in the CIV$\lambda1549_{\rm BC}$ (units as in Col. 3); Cols. 6, 7, 8 – centroid profile shift at $\frac{1}{4}$ maximum ($c(\frac{1}{4})$) followed by the estimated uncertainties on the blue and red wings of the profile (units km s^{-1}); Cols. 9, 10,11 – same at half-maximum ($c(\frac{1}{2})$, which is an adopted 4DE1 parameter); Cols. 12, 13 – centroid at $\frac{3}{4}$ maximum ($c(\frac{3}{4})$) with symmetric uncertainty ; Cols. 14, 15 – centroid at the 90% intensity level of the CIVλ1549 broad line (c(0.9)), with symmetric uncertainty; Cols. 16, 17 – FWHM(CIV$\lambda1549_{\rm BC}$) and estimated uncertainty (units km s^{-1}); Cols. 18,19, 20 – CIV$\lambda1549_{\rm BC}$ asymmetry index with estimated uncertainties on the blue and red profile wings; Cols. 21,22 – CIV$\lambda1549_{\rm BC}$ kurtosis measure and estimated uncertainty.

No CIV$\lambda1549_{\rm NC}$ measures are given in Table 2 if the profile if affected by partial (a)

or strong (A) absorption. In sources labeled a in Tab. 2 residual CIVλ1549$_{\rm NC}$ is sometimes visible but the NC width and flux cannot be recovered. NC shifts and fluxes are accurate (within $\pm$ 40% at a 2-σ confidence level) only if CIVλ1549$_{\rm NC}$ emission shows an intensity at least 0.05 CIVλ1549$_{\rm BC}$. Note that our adopted CIVλ1549$_{\rm NC}$ component is often not "[OIII]$\lambda\lambda$4959,5007-like". It is often significantly broader and stronger than would be subtracted if we used [OIII]λ5007 as a template for the CIVλ1549 doublet. See §4 for both empirical and theoretical justifications for our procedure.

Measured centroids at different fractional intensities were defined as follows:

$$c(\tfrac{i}{4}) = \frac{\lambda_{\rm B} + \lambda_{\rm R} - 2\lambda_0}{2\lambda_0}\, c, \forall i = 0, \ldots 4, \tag{1}$$

where c is the speed of light. Values $c(\frac{i}{4})$ for $i = 0$ are not listed in Tab. 2 due to the difficulty of assessing $\lambda_{\rm B}$ and $\lambda_{\rm R}$ at zero intensity. We give $c(\frac{9}{10})$ instead of peak radial velocity. This has been shown to be a good surrogate and less dependent on CIVλ1549$_{\rm NC}$ subtraction as well as line profile irregularities (Marziani et al. 2003a). The asymmetry index is defined as follows:

$$A.I. = \frac{\lambda_{\rm B}(\frac{1}{4}) - \lambda_{\rm R}(\frac{1}{4}) - 2\lambda_{\rm P}}{\lambda_{\rm P}} \tag{2}$$

where for $\lambda_{\rm P}$ we use $c(\frac{9}{10})/c$. The kurtosis index is defined as:

$$kurt = \frac{\lambda_{\rm R}(\frac{3}{4}) - \lambda_{\rm B}(\frac{3}{4})}{\lambda_{\rm R}(\frac{1}{4}) - \lambda_{\rm B}(\frac{1}{4})} \tag{3}$$

(cf. Marziani et al. 1996).

Uncertainties reported in Tab. 2 were estimated by measuring the wavelengths $\lambda_{\rm R}$ and $\lambda_{\rm B}$ at $\pm$ 5% fractional intensity and then quadratically propagating the errors in the relationships reported above. All uncertainties reported in Table 2 represent a 2σ confidence level. Uncertainties in estimating the rest frame velocity, relative to which the centroids are computed, can be as large as 300 km s^{-1} or as small as $\sim$ 30 km s^{-1} (at 1σ confidence level) depending on the availability of moderate resolution spectra (SDSS is, or will be, improving the situation for about 50% of the sample). The error in estimating the local rest frame $\Delta z \approx 0.00014 \pm 0.0006$ was derived from the distribution of differences between z values used in this work and those given in NED. Combining the typical uncertainty on systemic velocity, on UV wavelength calibration, and the average of the measurement uncertainty reported in Table 2, the typical uncertainty (at a 2-σ confidence level) are $\approx$ 230 km s^{-1}and $\approx$ 170 km s^{-1} for $c(\frac{1}{2})$ and $c(\frac{3}{4})$.

2.3. CIVλ1549 Line Parameters in the RQ-RL Context

Figure 2 shows source occupation in 4DE1 planes involving the $c(\frac{1}{2})$ parameter (as defined in Sulentic et al. 2000b). $c(\frac{1}{2})$ was chosen from among possible CIVλ1549 profile measures (FWHM, $c(\frac{1}{2})$ and equivalent width) because: 1) it is not obviously luminosity dependent, 2) it showed the largest intrinsic dispersion and 3) it showed possible correlations with the other principal 4DE1 parameters. As a luminosity normalized measure W(CIVλ1549$_{\rm BC}$) is ruled out even if the well-known "Baldwin effect" now appears to be driven by dependance on the Eddington ratio (Bachev et al. 2004; Baskin & Laor 2004). This does not mean that we regard it as an unimportant measure but only that we reject it as one of the principal 4DE1 parameters. A surrogate measure might involve a direct measure of CIVλ1549$_{\rm BC}$ line flux but the parameter dispersion of that measure is less than for $c(\frac{1}{2})$. The same is true for FWHM(CIVλ1549$_{\rm BC}$) which also shows less dispersion than FWHM(H$\beta_{\rm BC}$). Line broadening may be due to both rotational and non-rotational velocity components especially if a disk + wind model is applicable to our sources. $c(\frac{1}{2})$ on the contrary, is most likely related to the amplitude of any non-virial motions in the BLR. It is this parameter that adds a new element that can be argued to be *physically orthogonal* to previously defined E1 parameters: FWHM(H$\beta_{\rm BC}$) estimates the virial broadening in the LIL-emitting part of the BLR; $R_{\rm FeII}$ measures the ionization conditions, while $\Gamma_{\rm soft}$ provides a measurement of the continuum shape.

RQ and RL sources are indicated by circles and squares respectively in Fig. 2 (sources with radio/optical flux ratio log R$_K \gtrsim 1.8$ are considered RL: Sulentic et al. 2003). The large number of squares reflects the over-representation of RL sources in our sample. Figure 2a shows that sources with CIVλ1549 profile blueshifts strongly favor RQ AGN with FWHM H$\beta_{\rm BC} \lesssim$ 4000 km s^{-1}. RL sources show a large scatter of both red and blue CIVλ1549 shifts. Figures 2bc show that sources with CIVλ1549 blueshift especially favor RQ sources with large $R_{\rm FeII}$ (strong optical FeII emission) and $\Gamma_{\rm soft}$ (a soft X-ray excess) measures respectively. RL sources are much more strongly concentrated in the latter two 4DE1 planes.

Table 3 gives mean parameter values (sample standard deviations in parenthesis) for total sample, RQ, RL and our previously defined Pop. A-B subsamples that will be considered in the next section. Values are given for: Col. 2 – number of sources; Col. 3 – equivalent width measure of the CIVλ1549$_{\rm BC}$ line; Col. 4 – $c(\frac{1}{2})$ of CIVλ1549$_{\rm BC}$; Col. 5 – FWHM(CIVλ1549$_{\rm BC}$); Col. 6 – FWHM(H$\beta_{\rm BC}$); Col. 7 – $R_{\rm FeII}$ and Col. 8 – $\Gamma_{\rm soft}$. Columns 4,6,7 and 8 represent the principal parameters in 4DE1. We find that RL sources show broader H$\beta_{\rm BC}$ and CIVλ1549$_{\rm BC}$ profiles than RQ AGN while RQ sources show stronger $R_{\rm FeII}$, $\Gamma_{\rm soft}$ and $c(\frac{1}{2})$ (blueshift) than the RL sample. FWHM CIVλ1549$_{\rm BC}$ is on average (17%) broader than FWHM H$\beta_{\rm BC}$ for RQ sources while FWHM H$\beta_{\rm BC}$ is (16%) narrower

than FWHM CIVλ1549$_{\rm BC}$ for RL sources. These differences relate to one of the most significant results of our earlier work where a restricted optical domain space occupation was found for RL sources. Figure 2 also shows this restricted occupation as a strong concentration of RL sources in a small region of the $c(\frac{1}{2})$ vs. $R_{\rm FeII}$ and $\Gamma_{\rm soft}$ planes. RL sources are rarely found with 4DE1 parameter values: FWHM(H$\beta_{\rm BC}$) $\lesssim$4000 km s^{-1}, $R_{\rm FeII}\gtrsim$ 0.3, $\Gamma_{\rm soft}\gtrsim$2.5 and $c(\frac{1}{2})\lesssim$0 km s^{-1}. The expanded CIVλ1549 sample confirms and strengthens this result which likely indicates a fundamental difference in BLR structure, kinematics and/or physics between RL and RQ populations (see Sulentic et al. 2003, for discussion in the context of a RQ-RL dichotomy).

Spearman rank correlation coefficients and associated probabilities are given in Table 4 for CIVλ1549 equivalent width, FWHM and centroid measures versus the three other principal 4DE1 parameters. The total-sample correlation coefficients for this sample are larger than corresponding values given for the smaller sample of sources in Sulentic et al. (2000b) as one might hope to see if the correlations are in some sense real. Table 4 emphasizes the spectroscopic differences between RQ vs RL sources by showing no evidence for correlations among 4DE1 parameters for RL sources. Real or marginal correlations are only found among RQ sources with the strongest correlations involving $c(\frac{1}{2})$, $R_{\rm FeII}$ and $\Gamma_{\rm soft}$. Restriction to a BG92 overlap subsample shows no significant difference in correlation coefficients.

3. Evidence for Two Populations of Broad Line AGN

So far we have compared sources on the conventional basis of a RQ vs. RL dichotomy however it is important to point out that about 25% of RQ sources in our sample occupy the same 4DE1 parameter domain as the RL AGN. If 4DE1 parameters reflect broad line physics/kinematics then this overlap may be important. The restricted 4DE1 parameter space occupation for RL sources motivated us (Sulentic et al. 2000b) to hypothesize the existence of two AGN "populations" (A and B) defined in an optical spectroscopic context (4DE1) rather than on the basis of radio loudness. Following our scheme Population A sources show FWHM(H$\beta_{\rm BC}$) $\lesssim$ 4000 km s^{-1}, strong $R_{\rm FeII}$, strong $\Gamma_{\rm soft}$ (a soft X-ray excess) and a $c(\frac{1}{2})$ blueshift with estimated probability of radio loudness $P\lesssim 0.01$. Population B sources show FWHM(H$\beta_{\rm BC}$) $\gtrsim$ 4000 km s^{-1}, weak $R_{\rm FeII}$, no soft X-ray excess or CIVλ1549 blueshift with estimated probability of radio loudness $P\approx$0.30. Revisiting Fig. 2a in the population A-B context shows that CIVλ1549 blueshifts are strongly concentrated among Pop. A sources with FWHM(H$\beta_{\rm BC}$) $\lesssim$ 4000 km s^{-1}. Filled and open symbols in Figures 2 identify Pop. A and B sources respectively. It is important to point out that FWHM(H$\beta_{\rm BC}$) = 4000 km s^{-1} was chosen as a Pop. A-B boundary before $c(\frac{1}{2})$ was selected as an 4DE1

parameter. Pop. A-B is more effective than the RQ-RL distinction for highlighting spectroscopic differences.

Pop. B sources show a scatter of line shifts within $c(\frac{1}{2}) = \pm$ 2000 km s^{-1} (Table 2) with mean value in Table 3 consistent with zero shift. A large part of the Pop. B scatter may be associated with CIVλ1549 measurement uncertainties (the 3σ shift uncertainty is $\approx$ 400 km s^{-1}). Fig. 2 show that Pop. A sources have a wider parameter dispersion than Pop. B sources. The majority of Pop. B sources are so concentrated that one can assign unique (within measurement errors) values of $R_{\rm FeII}\sim$ 0.15 $\pm$ 0.15 and $\Gamma_{\rm soft}\approx$ 2.1$\pm$ 0.5. to the entire population. These two values along with $c(\frac{1}{2})$ = –70 (consistent with 0) $\pm$ 1000 km s^{-1} represent the 4DE1 coordinates with highest probability of radio-loudness.

The strong parameter concentration of Pop. B sources relative to the Pop. A RQ majority reenforces the interpretation (Sulentic et al. 2003) that RL quasars represent a distinct AGN population and perhaps the endpoint of quasar activity in sources with largest $M_{\rm BH}$ and lowest $L_{\rm bol}/L_{\rm Edd}$. The obvious question then involves the relationship between Pop. B RQ sources and Pop. B RL AGN. RL and RQ Pop. B sources show strong similarity in most properties but $c(\frac{1}{2})$ suggests a possible small separation with mean CIV$\lambda1549_{\rm BC}$ shift values of about –200 and +70 km s^{-1} respectively for Pop. B RQ and RL sources. However both values are consistent with zero shift given measurement uncertainties. A $K-S$ test for the two $c(\frac{1}{2})$ distributions confirms no significant difference. If CIV$\lambda1549_{\rm BC}$ blueshift and negative asymmetry index are the signature of a disk wind that is driven by high $L_{\rm bol}/L_{\rm Edd}$ then 60-80% of RQ and very few RL, sources show evidence for it. RQ sources in our sample have an average negative asymmetry index (–0.1), and a K-S test confirms a significant difference with the distribution for RL sources (whose average is +0.08). The simplest answer to the above question then would be that for a given $M_{\rm BH}$, RL sources lie at the extreme low end of an $L_{\rm bol}/L_{\rm Edd}$ sequence – perhaps they are expiring quasars. Perhaps Pop. B RQ sources with lowest values of CIV$\lambda1549_{\rm BC}$ shift are the RQ expiring quasars. In that case our population B designation has a physical significance although we do not yet know what physical property allows/inhibits radio loud activity.

3.1. Population A and NLSy1s

The distinction between Pop. A and B may be more fundamental than RQ-RL or NLSy1-BLSy1. Fig. 2 shows that CIVλ1549 blueshifts are equally divided between sources with FWHM(H$\beta_{\rm BC}$) $\lesssim$ 2000 km s^{-1} (traditional NLSy1) and sources with FWHM(H$\beta_{\rm BC}$) in the range 2000–4000 km s^{-1} (BLSy1). A K-S test reveals no significant distribution difference between the two groups of sources suggesting that the 2000 km s^{-1} cutoff for NLSy1 is

artificial. The same is true for comparisons involving W(CIVλ1549$_{\rm BC}$), FWHM(CIVλ1549) and $\Gamma_{\rm soft}$ parameter distributions. Only $R_{\rm FeII}$ seems shows possible evidence for a difference ($D_{\rm KS} \approx 1.65$ with probability $P \approx 0.01$ that the two $R_{\rm FeII}$ data sets are not drawn from the same parent population). Caution is needed because the precision of the $R_{\rm FeII}$ measure depends in both S/N and the line width (Marziani et al. 2003a). Considering the similarity in $\Gamma_{\rm soft}$ and CIVλ1549 centroid shifts (which are likely related accretion rate and disk wind properties) the Pop. A/B distinction can be viewed as a physically motivated re-definition of the NLSy1/BLSy1 boundary originally introduced by Osterbrock & Pogge (1985) and subsequently adopted by 4DE1 for different (RL) reasons.

3.2. Population Subdivision and Quasar Structure

Tables 3 and 4 show that the Pop. A-B discrimination is more effective than the RQ-RL distinction for emphasizing source differences. Table 3 shows that almost all sample mean differences between Pop. A and Pop. B are *larger* than equivalent differences between RQ and RL. Since the entire RQ source population shows a larger parameter spread than Pop. A RQ sources alone, it should be *more* sensitive to correlation than Pop. A RQ alone. Table 4 confirms that in no case does the entire RQ sample show a higher correlation coefficient than Pop. A sources alone. In all cases the correlation coefficient improves (or remains the same) when we restrict the RQ sample to Pop. A RQ alone. We interpret these results as support for our hypothesis that the Pop. A-B distinction is *more fundamental* than the RQ-RL one. So far we have distinguished between Pop. A and B sources using FWHM H$\beta_{\rm BC}$ alone. The mean values given in Table 3 allow us to give best estimates for the Pop. A-B boundary using the other three principal 4DE1 parameters: $R_{\rm FeII} \approx 0.4$, $\Gamma_{\rm soft} \approx 2.60$ and $c(\frac{1}{2}) \approx 0$ km s^{-1}.

1D projections of the 4DE1 space like Fig. 2abc show a main sequence of source occupation/correlation. The Population A-B concept reflects either a continuous variation in physical/geometric/kinematic properties along this sequence or a true source dichotomy possibly driven by a critical value of $L_{\rm bol}/L_{\rm Edd}$ (with Pop. B RQ-RL dichotomy due perhaps to BH spin, host galaxy properties and role for secular evolution in BH growth). In the former case Pop. A-B remain useful as a vehicle for emphasizing source extrema providing a valuable challenge to models of BLR structure/kinematics as well as changes in them due to physics and/or source evolution (Marziani et al. 2001, 2003b; Boroson 2002). In the past few years we have favored the possibility of two disjoint AGN populations on the basis of multifold evidence:

- A possible gap or paucity of sources with FWHM(H$\beta_{\rm BC}$) $\approx$ 4000 km s^{-1}, which is

appreciable also in e.g., Fig. 6 of Wang et al. (1996), Fig. 2 of Boller (2004), in Fig. 1 of Sulentic et al. (2000b), in Fig. 3 of (Baskin & Laor 2005), most impressively in Figure 7 (right panel) of (Corbin & Boroson 1996) and see also Collin et al. (2006).

- Most RL sources lie above FWHM H$\beta_{\rm BC} \approx 4000$ km s^{-1} while most RQ sources lie below this value. The few RL with FWHM H$\beta_{\rm BC} \lesssim 4000$km s^{-1} are likely viewed at an orientation that minimizes any rotational component associated with BLR motions (Sulentic et al. 2003, they fall there because of orientation rather than physics).

- Sources with FWHM(H$\beta_{\rm BC}$) $\lesssim 4000$ km s^{-1} show average profiles well fit by a Lorentzian function while broader line sources show profiles that are frequently red-ward asymmetric and that require two Gaussians for a reasonable fit (Sulentic et al. 2002).

- Sources with FWHM(H$\beta_{\rm BC}$) $\lesssim 4000$ km s^{-1} often show a soft X-ray excess ($\Gamma_{\rm soft} \gtrsim 2.8$) while those above this limit almost never show one (Boller 2004; Sulentic et al. 2000a).

- Sources with weak (usually less than 10 Å equivalent with) and blueshifted [OIII]λ5007 (the so-called blue outliers) are found only in sources with FWHM(H$\beta_{\rm BC}$) $\lesssim$ 4000 km s^{-1} (Zamanov et al. 2002; Marziani et al. 2003b).

- All sources with CIVλ1549 $c(\frac{1}{2}) \lesssim$ –3000 km s^{-1} show FWHM H$\beta_{\rm BC} \lesssim$4000 km s^{-1} (Fig. 2a). Most sources with CIVλ1549 $c(\frac{1}{2}) \lesssim$ –1000 km s^{-1} also lie below the same FWHM limit. Sources with broader H$\beta_{\rm BC}$ show a scatter of values between CIVλ1549 $c(\frac{1}{2})\pm$ 2000km s^{-1}. W(CIVλ1549) measures also show a strong difference (not correlation) in mean values for source greater and less than FWHMH$\beta_{\rm BC} = 4000$ km s^{-1}.

- Comparison of CIVλ1549 and H$\beta_{\rm BC}$ profiles suggest a discontinuity at FWHM(H$\beta_{\rm BC}$)$\approx$ 4000 km s^{-1}. FWHM(H$\beta_{\rm BC}$) and FWHM(CIVλ1549$_{\rm BC}$) are correlated above this value but not below (Marziani et al. 1996; Baskin & Laor 2005, see also Table 4).

- Fig. 3 shows a possible new correlation between CIVλ1549 FWHM and $c(\frac{1}{2})$ measures. Comparison of Fig. 3a and 3b for Pop. B and A sources, respectively, indicates that the correlation exists only for sources with FWHM(H$\beta_{\rm BC}$) $\lesssim$4000 km s^{-1} (Pop. B sources show a scatter diagram) . This CIVλ1549 inter-correlation for Pop. A sources shows a reasonably strong correlation (corr. coeff. ≈ 0.5). The best fit relation is $c(\frac{1}{2})$(CIVλ1549$_{\rm BC}$) = 963 – 0.426 FWHM(CIVλ1549$_{\rm BC}$) [km s^{-1}].

The correlation in Fig. 3 might be expected from (and constraining of) models that view Pop. A sources as the highest accreting AGN that generate a disk wind (Murray et al. 1995; Bottorff et al. 1997; Proga & Kallman 2004). Previous results may also indicate a change in

BLR structure perhaps at a critical value of $L_{\rm bol}/L_{\rm Edd}$ (corresponding to FWHM(H$\beta_{\rm BC}$) $\approx$ 4000 km s^{-1}) with an accretion disk + outflowing high-ionization wind required to explain Pop. A source measures (Marziani et al. 1996, 2001, 2003a). Pop. B sources do not allow us to rule out the possibility of a single stratified emission region producing both LILs and HILs. Pop. A and B sources differ in almost every mean property that can be defined. Table 5 summarizes both phenomenological differences (mean values given where available) as well as some physical differences (preceded by •) that can be inferred from the empiricism. Note that not all of the cited works make a distinction between Pop. A and B.

Table 3 shows that W(CIVλ1549$_{\rm BC}$) differs by a factor of $\approx$ 2 between Pop. A and B sources, with Pop. A sources showing lower values. Since Pop. A and B do not show a significant difference in mean source luminosity (Bachev et al. 2004) we ascribe the EW difference to a difference in $L_{\rm bol}/L_{\rm Edd}$which is known to be stronger than the luminosity dependence (Bachev et al. 2004; Baskin & Laor 2004). Pop. A and B differ systematically in $L_{\rm bol}/L_{\rm Edd}$, as shown by Marziani et al. (2003b, 2006). While not a principal 4DE1 parameter it is clear that W(CIVλ1549$_{\rm BC}$) is an important measure.

4. CIVλ1549 Narrow Line Emission

All tabulated parameter means and correlation coefficients discussed above depend upon proper processing of the CIVλ1549 spectra. Confusion exists about the reality and strength of a narrow line CIVλ1549 component (CIVλ1549$_{\rm NC}$) presumably arising from the same narrow-line region (NLR) as e.g. [OIII]$\lambda\lambda$4959,5007 and narrow Hβ. There is now no doubt that CIVλ1549$_{\rm NC}$ emission is common in AGN (see also Sulentic & Marziani 1999). High and low redshift type 2 AGN with obvious CIVλ1549$_{\rm NC}$ emission have recently been found in significant numbers: Barger et al. (2002); Jarvis et al. (2005)(*); Norman et al. (2002)(*); Stern et al. (2002)(*); Szokoly et al. (2004); Mainieri et al. (2005)(*); Severgnini et al. (2006). According to Meiksin (2006) only four confirmed high redshift (z >1.6) type 2 AGN are known (refs. marked with * above). All four show prominent CIVλ1549$_{\rm NC}$ (see also Dawson et al. 2001).

In contrast to Hβ a clear, unique NLR/BLR inflection is less often seen in the CIVλ1549 profiles making NLR correction less certain. This is not surprising when one considers that the intrinsic velocity resolution at CIVλ1549 is 3 times lower than at Hβ. NLR CIVλ1549 can also be broader than other narrow lines because: a) it is a doublet with $\Delta v \approx$ 500 km s^{-1} and b) it can arise in denser than average parts of the NLR (as for ø4363; e.g. Marziani et al. 1996; Sulentic & Marziani 1999). We argue that cautious subtraction of a suitable narrow component is essential for exploiting the information content in the CIVλ1549

line (see Bachev et al. 2004). We subtracted a significant (W > 1 Å) NLR component from 76/130 sources in this sample. Figure 1 shows the individual CIVλ1549 profiles with narrow components indicated in order to assist visual assessment of the component on a source-by-source basis.

Baskin & Laor (2005) recently pointed out that our earlier CIVλ1549$_{\rm BC}$ and CIVλ1549$_{\rm NC}$ measurements (Marziani et al. 1996) were "non-unique". Every experimental measure is non-unique and the lack of uniqueness is customarily indicated by error bars. Rather than uniqueness, the question we are addressing is whether or not there is a significant narrow component in the CIVλ1549 line. The second question, assuming that such a component is present, involves how accurately we can measure it. The third question, assuming we can accurately measure it, is whether correction for CIVλ1549$_{\rm NC}$ matters. The goals of this section are to provide a recipe for consistent CIVλ1549$_{\rm NC}$ correction and to show that very different results emerge from corrected CIVλ1549 measures.

The strong and relatively narrow core (FWHM $\lesssim$ 2000 km s^{-1}) observed in many CIVλ1549 profiles was previously noted and an *ad hoc* intermediate line region (ILR) was introduced in order to account for it (Brotherton et al. 1994; Brotherton & Francis 1999). The ILR was defined as having some properties typical of the canonical BLR necessitating the postulation of an additional VBLR component in order to explain the broad wings often seen in CIVλ1549 spectra (e.g. Figure 1). Unfortunately the ILR approach is not fully consistent because narrow CIVλ1549 cores are significantly narrower than corresponding H$\beta_{\rm BC}$ profiles (Sulentic & Marziani 1999) which are a canonical BLR feature. They are sometimes as narrow as the [OIII]λ5007 lines. Intermediate ionization lines of CIII]λ1909 and SiIII]λ1892 measured in average spectra (Bachev et al. 2004) show widths that are more consistent with H$\beta_{\rm BC}$ and much broader than the narrow cores of CIVλ1549 that we ascribe to the NLR. In addition density-sensitive ratios measured near the CIII]λ1909 blend are consistent with BLR density ($n_{\rm e} \sim 10^{10}$ cm^{-3}: see Brotherton et al. (1994); Bachev et al. (2004)). This reinforces our interpretation that the hypothesized ILR+VBLR components as simply the more canonical NLR+BLR. The larger width of CIVλ1549$_{\rm NC}$ compared to H$\beta_{\rm NC}$ or [OIII]λ5007 can be easily explained within the framework of a density/ionization gradient within the NLR, as further described below.

Almost all other studies of CIVλ1549 line properties (Wills et al. 1995; Corbin & Boroson 1996; Wills et al. 1999; Vestergaard 2002; Warner et al. 2004) do not subtract CIVλ1549$_{\rm NC}$ emission. Baskin & Laor (2005) assume that the width and strength of CIVλ1549$_{\rm NC}$ and [OIII]λ5007 are correlated. In most cases this implies that the ratio CIVλ1549/[OIII]λ5007 is $\lesssim 1$. The physical relationship between forbidden [OIII]$\lambda\lambda$4959,5007 and permitted CIVλ1549$_{\rm NC}$ is however unclear leaving little basis for assuming a fixed relation. The

[OIII]$\lambda\lambda$4959,5007 lines often show a strong blue wing that might be described as a semi-broad component. So-called blue outlier sources show this component and it is expected to be a *strong* CIVλ1549 emitter (Zamanov et al. 2002). Our analysis suggests that CIV$\lambda1549_{\rm NC}$ is likely absorbed by dust or is intrinsically weak in $\approx 50\%$ of sources. Among the remainder about 1/3 of the sources show CIV$\lambda1549_{\rm NC}$ significantly broader than narrow Balmer and [OIII]$\lambda\lambda$4959,5007 emission. It is probably emitted by a reddening-free high-density (or high-ionization) innermost region of the NLR. Whatever its origin and relationship to other narrow lines it is present in the spectra of many sources and will affect our efforts to parameterize CIV$\lambda1549_{\rm BC}$.

The motivation for relatively high density emission in the NLR stems from the clear evidence of relatively large CIV$\lambda1549_{\rm NC}$/[OIII]λ5007 intensity ratios in several sources: NGC 5548, NGC 7674 and I Zw 92 (Kraemer et al. 1994, 1998), with CIV$\lambda1549_{\rm NC}$/[OIII]$\lambda5007 \approx 2$. Also, even if Baskin & Laor (2005) subtracted little CIV$\lambda1549_{\rm NC}$, the average non-zero subtraction for the 16 sources in common with the present study implies CIV$\lambda1549_{\rm NC}$/[OIII]$\lambda5007$ ≈ 0.3. This value already indicates bulk emission from $\log n_{\rm e} \gtrsim 5.5$, much above the "standard" NLR density $n_{\rm e}\sim 10^4$ cm^{-3}. The CIVλ1549/[OIII]λ5007 intensity ratio increases with density around the [OIII]$\lambda\lambda$4959,5007 critical density because of the drastic collisional quenching that suppresses [OIII]$\lambda\lambda$4959,5007 but not CIVλ1549. The observed FWHM differences between [OIII]$\lambda\lambda$4959,5007, H$\beta_{\rm NC}$, and CIV$\lambda1549_{\rm NC}$ are recovered under standard assumptions if a density gradient is assumed for the NLR, with $3 \lesssim \log n_{\rm e} \lesssim 7 \div 8$ (Sulentic & Marziani 1999).

We suggest the following CIV$\lambda1549_{\rm NC}$ subtraction procedure as the most reliable way to obtain reasonable and reproducible CIV$\lambda1549_{\rm NC}$ measures.

Step 1: Inflection Sources showing a CIVλ1549 NLR/BLR inflection can be treated the same as Hβ as long as the width/shift/intensity constraints given below are not violated. See the profiles in Figure 1 and Appendix A discussion of PG 0026+126 which shows a strong profile inflection. There was no simultaneous fitting. The underlying CIV$\lambda1549_{\rm BC}$ was fit with an high-order spline function. The overlying narrow component was set by bordering the fitting range at inflection points which defined a core that met the FWHM and flux ratio criteria described below. The FWHM was measured using a Gaussian fit, or by measuring the half-maximum wavelengths if the profile was absorbed or very different from Gaussian.

Step 1a: No Inflection or Multiple Inflections Most sources do not show an inflection or sometimes show multiple inflections between reasonable limits of width and strength. This motivates us to set a conservative limit on FWHM CIV$\lambda1549_{\rm NC}$. Simple models suggest that lines like CIVλ1549 can be significantly broader than [OIII]λ5007

(Sulentic & Marziani 1999). CIVλ1549 lines with FWHM $\lesssim$ 1500 km s^{-1} are now observed in higher redshift type-2 AGN (see above references). We therefore suggest subtracting a CIVλ1549$_{\rm NC}$ component with FWHM $\leq$ 1500 km s^{-1} again subject to shift and intensity constraints that follow (see Fig. 6). In just two cases (3C 110 and 3C 273) our data suggested a somewhat broader component but inclusion/exclusion of these few sources as processed, or reduction of the NLR component to this limit will not affect the main conclusions of this study. The choice was usually to maximize the CIVλ1549$_{\rm NC}$ FWHM within the flux ratio condition as described below. Any narrow feature with FWHM $\lesssim$ 900 km s^{-1} has no physical meaning. The feature we identify as CIVλ1549$_{\rm NC}$ shows FWHM $\approx$ 1200 $\pm$ 300 km s^{-1}in 95% of sources with significant narrow emission (Fig. 6).

Step 2: Nebular Physics and Observations There is no strong upper limit for the expected CIVλ1549/[OIII]λ5007 intensity ratio in the absence of internal dust extinction. Both high ionization and high density can produce an arbitrarily large ratio (Contini & Viegas 2001; Kraemer et al. 1998; Baldwin et al. 1995). We adopt CIVλ1549/[OIII]λ5007 $\approx$ 10, derived for the high-ionization region of NGC 5548 (Kraemer et al. 1998), as a *strict* upper limit. Using again observational results as a guideline, we consider Seyfert 1 sources in our sample that show prominent, unambiguous CIVλ1549$_{\rm NC}$ (NGC sources, PKS 0518-45, and 3C 390.3). We find a large dispersion in the reddening-corrected CIVλ1549$_{\rm NC}$/[OIII]λ5007 ratio with a mean value $\approx$ 2 and a maximum $\approx$ 5 (NGC 3783). Therefore we can safely regard an CIVλ1549$_{\rm NC}$/[OIII]λ5007 intensity ratio $\approx$ 5 as an observationally defined boundary. If this condition is appropriate the ($A_{\rm B}$ corrected) distribution of CIVλ1549/[OIII]λ5007 intensity ratios (shown in Fig. 6) does not pose any special challenge, including the few sources for which 5 $\lesssim$ CIVλ1549$_{\rm NC}$/[OIII]λ5007 $\lesssim$ 10 (with an uncertainty of $\pm$ 50% these sources are not significantly above our adopted limit of 5).

Step 3: NLR shift In most sources the [OIII]λ5007 and/or H$\beta_{\rm NC}$ profile centroid is used to define the rest frame of a source. Limited available HI and CO measures of host galaxy emission support this definition except for a few extreme Pop. A (some but not all formally NLSy1s) blue outlier sources. We use the peak of Hβ to define the source rest frame of blue outliers. The CIVλ1549$_{\rm NC}$ profile centroid (Table 2) agrees with the optically defined rest frame in most sources. Ninety percent of our sources show a CIVλ1549$_{\rm NC}$ centroid within $\pm$400km s^{-1}. This is reasonable considering that the average FWHM(CIVλ1549$_{\rm NC}$) =1120 km s^{-1} and that CIVλ1549$_{\rm NC}$ is strongly sensitive to S/N. Shifts of several hundred km s^{-1} are occasionally observed and may be due to: a) an intrinsic CIVλ1549$_{\rm NC}$ blueshift, b) narrow-line absorption that creates a spurious shift to the red (and, indeed, inspection of Fig. 1 reveals that this is the case

for most sources where CIVλ1549$_{\rm NC}$ appears to be significantly redshifted) and c) poor rest frame determination. However only 5 sources out of 29 with $|\Delta v_{\rm r}|$(CIVλ1549$_{\rm NC}$) $\gtrsim$ 300 km s^{-1} show a $\Delta z \approx \pm$ 0.001.

Figure 6 summarizes our CIVλ1549$_{\rm NC}$ measures: line luminosity distribution of CIVλ1549$_{\rm NC}$ (upper right); distribution of CIVλ1549$_{\rm NC}$/[OIII]λ5007 luminosity ratios (lower left); distribution of CIVλ1549$_{\rm NC}$ FWHM measures (upper right); distribution of CIVλ1549$_{\rm NC}$ measures in the line luminosity–FWHM plane (lower right). Application of above procedures resulted in a subtracted NLR component usually less than W(CIVλ1549$_{\rm NC}$) $\approx$ 10 Å but with a few extreme cases usually low luminosity Seyfert 1's. RL sources show the largest fraction of detectable CIVλ1549$_{\rm NC}$ components (0.71) compared to 0.48 for RQ AGN. Our Pop. B sources show a slightly larger fraction of CIVλ1549$_{\rm NC}$ components (0.63) than Pop. A (0.51). Some sources do not allow an unambiguous CIVλ1549$_{\rm NC}$ subtraction with a significant range of acceptable solutions. This ambiguity and its effect on CIVλ1549$_{\rm BC}$ are usually within the adopted errors (even if the effect on CIVλ1549$_{\rm NC}$ is much larger), that have been estimated changing the fractional intensity levels by $\pm$5%. As described earlier, the random scatter in Galactic line radial velocity after realignment is just $\approx$ 40 km s^{-1}. Therefore it is possible that several CIVλ1549$_{\rm NC}$ shifts are significant because they show values larger than the expected calibration and measurement uncertainties. Examining spectra in Fig. 1 one will occasionally see a CIVλ1549 profile with a peak as narrow as some subtracted CIVλ1549$_{\rm NC}$ (e.g. J13253−3824 and J15591+3501). In these cases subtraction of the sufficiently narrow peak would violate other selection rules (e.g. in the above two cases CIVλ1549$_{\rm NC}$/[OIII]λ5007$\gg$ 10). Note that we also verified *a posteriori* that the CIVλ1549$_{\rm NC}$ FWHM was less than FWHM(H$\beta_{\rm BC}$).

4.1. The Narrow Cores of CIVλ1549 Do Not Reverberate

An ideal check on our NLR results would involve reverberation mapping where any NLR component would be expected to remain stable. One IUE based study (Turler & Courvoisier 1998) reported PCA analysis on 18 AGN with 15 or more independent spectra. Ten of the sources are included in our sample. The principal component in their study was interpreted to involve the parts of the CIVλ1549 line profile that varied with zero lag time. The approach of Türler & Courvoisier was to isolate the principal component dominated by continuum and broad line variability. This was then subtracted from the mean spectrum to isolate the remaining information content (rest spectrum). Two things are seen in the rest spectrum: a narrow unshifted peak, and more complex and extended wings. The nature of the wings will depend upon the complexity and timescale of variations as well as the number and temporal

spacing of source spectra. Component 1 can be reasonably argued to be the NLR component of the line – the correlated intensity component that dominated our 2D analogy above.

In the case of 3C 273 only the continuum was present in the principal component. We identified and subtracted an NLR component in all ten overlap cases. A narrow component of similar strength and width is seen in the second principal component spectra for nine of these cases (except 3C 273). The least ambiguous case involves 3C 390.3 where there is a clear inflection between NLR and BLR. In that case agreement is perfect. Other sources like GQ Com, NGC 3783 and NGC 5548 also show strong agreement. The range of FWHM for the second principal component CIVλ1549 profiles 1-5000 km s^{-1} suggesting that the NLR is often blended with additional broad line emission. However, the overall agreement between the central cores and our own estimates of NLR CIVλ1549 emission gives us confidence that we have developed a reasonable approach to correcting the CIVλ1549 line profiles. The alternative is to ignore the problem which we argue will lead to spurious results.

4.2. Comparison with Previous Work

Other recent studies of the CIVλ1549 profile, using the same HST archival spectra, subtracted little (Baskin & Laor 2005) or no (Wills et al. 1993; Corbin & Boroson 1996; Vestergaard 2002; Kuraszkiewicz et al. 2002, 2004; Warner et al. 2004) NLR component. Figure 4 compares our CIV$\lambda1549_{\rm BC}$ FWHM and centroid shift ($c(\frac{1}{2})$) measures with equivalent values for sources in common with some of these studies. The LL panel of Figure 6 shows that Baskin & Laor (2005) subtracted a ($\sim$2-4 times) smaller and more constant NLR component. Direct comparison with Kuraszkiewicz et al. (2002, 2004) is not possible because they model the CIVλ1549 profile with multiple Gaussian components that do not correspond to our NLR and BLR interpretation. FWHM measures are strongly affected by under-subtraction of CIV$\lambda1549_{\rm NC}$. The UL panel of Figure 4 compares our FWHM CIV$\lambda1549_{\rm BC}$ measures with those of Baskin & Laor (2005) and Warner et al. (2004). Symbols for comparisons with Baskin & Laor (2005) (and Corbin & Boroson (1996)) retain the Pop. A-B and RQ/RL distinctions used in earlier figures. Our measures are systematically larger with the amplitude of Δ FWHM increasing systematically with FWHM CIV$\lambda1549_{\rm BC}$. The LL panel compares our FWHM measures with Corbin & Boroson (1996) and shows similar disagreement. Correlations such as FWHM Hβ vs. FWHM CIVλ1549 (Corbin 1991; Baskin & Laor 2005; Warner et al. 2004) found using uncorrected CIVλ1549 measures will likely be spurious except possibly for the Pop. B sources. The most striking evidence for correlation is found in Figure 7 (right) of Corbin & Boroson (1996) involving NC corrected H$\beta_{\rm BC}$ and uncorrected CIV$\lambda1549_{\rm BC}$ measures. One sees two groups of sources (pop. A

and B) each showing a positive trend but with different slopes for the two trends. The trends are displaced by Δ FWHM(CIVλ1549$_{\rm BC}$)=3000km s^{-1}at about FWHM(H$\beta_{\rm BC}$) = 4000km s^{-1}. The "Pop. B" trend can be described as displaced towards smaller values of FWHM(CIVλ1549$_{\rm BC}$). Since narrow line emission is systematically stronger in Pop. B (especially RL) sources we might expect those FWHM(CIVλ1549$_{\rm BC}$) measures to be more strongly affected by NC subtraction. Is the displacement entirely due to the lack of NC corrected FWHM(CIVλ1549$_{\rm BC}$) measures? Much of the displacement disappears in our equivalent FWHM-FWHM plot but the correlation seen for Pop. B sources ($r_{\rm S} \approx 0.5$) is stronger than for Pop. A ($r_{\rm S} \sim$0.3: not significant) and its extrapolation into the pop. A domain predicts much smaller (3000 km s^{-1}) values for FWHM(CIVλ1549$_{\rm BC}$) than are observed.

The right panels of Fig.4 compares our $c(\frac{3}{4})$ measures with those from Baskin & Laor (2005) (upper) and Corbin & Boroson (1996) (lower). There is a systematic displacement of uncorrected shift measures towards smaller or even redshifted values in both comparisons. This will tend to diminish the Pop. A-B (or RQ vs. RL) differences that are highlighted in this paper. The systematic CIVλ1549 blueshift for Pop. A sources becomes much less obvious using NC uncorrected CIVλ1549 measures and especially using shift measures taken closer to the profile peak (e.g., $c(0.9)$). Fig. 4 shows systematic differences between corrected and uncorrected measures that will erase or obscure important CIVλ1549 results like the ones discussed in this paper.

5. $M_{\rm BH}$ Calculations Using CIVλ1549 Width

CIVλ1549 has become the line of choice for black hole mass estimation in high- z quasars. It is a dangerous choice for at least two reasons: 1) it shows a systematic blueshift in many sources, and 2) FWHM CIVλ1549$_{\rm BC}$ does not correlate strongly or monotonically with FWHM H$\beta_{\rm BC}$ – the line of choice for low-redshift $M_{\rm BH}$ estimation. Reason 1 does not necessarily rule out a virialized distribution of emitting clouds but it certainly motivates caution when using the line to infer black hole mass. Blueshifted CIVλ1549 profiles are thought to arise in a high ionization wind resulting in a velocity flow that is not negligible relative to any rotational component (Murray et al. 1995; Proga & Kallman 2004). We think use of CIVλ1549 warrants even more caution because we see different line properties for Pop. A and B (or alternatively RQ and RL) sources. This raises the possibility that the geometry/kinematics of the CIVλ1549 emitting region may be fundamentally different in Pop. A and B sources. The population distinction is at least useful and possibly fundamental because it maximizes source differences. FWHM H$\beta_{\rm BC}$ and CIVλ1549$_{\rm BC}$ are most similar (Table 3) for RQ sources that show mean FWHM(CIVλ1549$_{\rm BC}$) only $\approx$600 km s^{-1} larger

than FWHM(H$\beta_{\rm BC}$). The RQ source distinction will therefore yield reasonable agreement between the two $M_{\rm BH}$ estimators. The same is true for sources under the RL distinction where FWHM(CIVλ1549$_{\rm BC}$) is $\approx$ 900 km s^{-1} broader. Both differences are approximately 15-16% of the mean RQ and RL profile widths respectively.

The two lines show larger difference when sources are divided using the Pop. A-B distinction where Δ FWHM (H$\beta_{\rm BC}$) – FWHM(CIVλ1549$_{\rm BC}$) $\approx$ –1900 km s^{-1} and $\approx$ +1400 km s^{-1} for pop. A and B respectively. These discrepancies amount to $\sim$56 % and $\approx$ 21 % of FWHM(CIVλ1549$_{\rm BC}$) + FWHM(H$\beta_{\rm BC}$)/2 for pop. A and B, respectively. This is larger than the measurement uncertainties for FWHM measures of both lines and further supports the utility of the pop. A-B concept. The two estimators will yield $M_{\rm BH}$ estimates that are more discrepant. Adopting the Pop. A-B distinction as more useful than the RQ-RL one then finds the largest Pop. A-B differences using FWHM(H$\beta_{\rm BC}$) where ΔFWHM (A-B) $\approx$ -4600 km s^{-1} compared to –1400 km s^{-1} using FWHM(CIVλ1549$_{\rm BC}$). The corresponding differences for the RQ-RL distinction are Δ FWHM (RQ–RL) $\approx$ –2800km s^{-1} (H$\beta_{\rm BC}$) and –1200 km s^{-1} (CIVλ1549$_{\rm BC}$).

As already pointed out (e. g., Marziani et al. 1996) the intrinsic dispersion of FWHM CIVλ1549$_{\rm BC}$ is less than for FWHMH$\beta_{\rm BC}$ making it less sensitive to differences between source populations. Since FWHM CIVλ1549$_{\rm BC}$ measures are less accurate than FWHM H$\beta_{\rm BC}$ values derived BH masses using the former will blur out any trends obtained with H$\beta_{\rm BC}$ measures. FWHM CIVλ1549$_{\rm BC}$ -derived masses will yield much larger $M_{\rm BH}$ estimates for Pop. A and smaller values for Pop. B. If one prefers to avoid the Pop. A-B distinction then one will find smaller CIVλ1549$_{\rm BC}$ – H$\beta_{\rm BC}$ differences using the RQ-RL distinction perhaps encouraging the incorrect assumption that a simple correlation exists between the two sets of $M_{\rm BH}$ measures. The smaller difference between mean FWHM values has also caused some to conclude that RQ and RL sources have similar $M_{\rm BH}$ distributions and mean values. Even if FWHM(CIVλ1549$_{\rm BC}$) could be measured with equal accuracy, and confidence about viriality, as FWHM(H$\beta_{\rm BC}$) it would be a less useful $M_{\rm BH}$ estimator because it shows less dispersion. The main source of disagreements about $M_{\rm BH}$ similarities and differences among AGN samples involves Pop. B RQ sources. Combining them with narrower lined RQ sources will raise the mean value of $M_{\rm BH}$ for that population with only small affect on the RL results. It will tend to equalize the means.

Estimates of $M_{\rm BH}$ were obtained from the UV flux density and FWHM CIVλ1549$_{\rm BC}$ reported in Table 2, as well as for the corresponding data from Baskin & Laor (2005) (their Table 1), assuming Hubble constant H_0 = 70 km s^{-1} Mpc^{-1} and relative energy density Ω_Λ = 0.7 and $\Omega_{\rm M}$ = 0.3. Values of $M_{\rm BH}$ were derived following the latest normalization of Vestergaard & Peterson (2006), which use the same cosmological parameters. The upper

panel of Figure 5 compares CIVλ1549 based $M_{\rm BH}$ estimates of Baskin & Laor (2005) (based on slightly CIV$\lambda1549_{\rm NC}$- corrected CIVλ1549 measures) with the NC-corrected estimates derived from this paper. We see that Baskin & Laor (2005) measures are systematically low and that the difference from our results increase with $M_{\rm BH}$. This comparison involves only sources in common between the two studies and involves only a 2dex range in $M_{\rm BH}$. The differences between our measures and completely uncorrected CIVλ1549 profiles will be larger. We note that both Pop. A and B sources show this disagreement. The middle panel of Fig. 5 compares $M_{\rm BH}$ measures based upon FWHM CIV$\lambda1549_{\rm BC}$ and H$\beta_{\rm BC}$. We show the ratio of CIV$\lambda1549_{\rm BC}$/H$\beta_{\rm BC}$ –derived $M_{\rm BH}$ measures as a function of H$\beta_{\rm BC}$–derived $M_{\rm BH}$. The H$\beta_{\rm BC}$ and continuum flux density measures come from Marziani et al. (2003a). The latest normalization of Vestergaard & Peterson (2006) was applied to these data, too.

We suggest a corrected FWHM(H$\beta_{\rm BC}$) measure (reduced by a fraction dependent on FWHM(H$\beta_{\rm BC}$)) as likely to be the most reliable virial estimator for reasons described in Sulentic et al. (2006a). The middle panel of Fig. 5 suggests that (NC corrected) CIVλ1549 based $M_{\rm BH}$ estimates for Pop. B sources are more consistent with ones computed from the corrected H$\beta_{\rm BC}$ width. However the scatter is large and our CIVλ1549 regression line is 0.2dex higher than for $M_{\rm BH}$ derived from H$\beta_{\rm BC}$. The most serious disagreement involves Pop. A sources ($\approx 60\%$ of RQ sources) which show a trend where the $M_{\rm BH}$ ratio increases with decreasing $M_{\rm BH}$. This does not allow one to easily correct CIVλ1549-computed $M_{\rm BH}$ to H$\beta_{\rm BC}$ values unless information on the optical spectrum (rest frame and H$\beta_{\rm BC}$ line width) is available. We made several attempts to deduce a correction for CIVλ1549-derived $M_{\rm BH}$ values from properties intrinsic to the CIVλ1549 profile shape (i.e., width, asymmetry and kurtosis) but were unable to find an effective relationship. Perhaps the most effective relationship we found involves the one shown in the lower panel of Fig. 5 which shows that the ratio of $M_{\rm BH}$ derived from CIVλ1549 and H$\beta_{\rm BC}$ is loosely correlated with W(CIV$\lambda1549_{\rm BC}$) (for W(CIV$\lambda1549_{\rm NC}$) $\lesssim 100$ Å). CIV$\lambda1549_{\rm BC}$ and H$\beta_{\rm BC}$ estimates of $M_{\rm BH}$ show better agreement for larger values of W(CIV$\lambda1549_{\rm BC}$). Caution is advised because equivalent width measures may be affected by continuum reddening. We also suffer from a relatively small sample of sources with W(CIV$\lambda1549_{\rm BC}$) $\gtrsim 100$ Å. Our fears about CIVλ1549–derived estimates for $M_{\rm BH}$ have motivated us to pursue Hβ to the highest possible redshift and we have recently presented H$\beta_{\rm BC}$ derived $M_{\rm BH}$ estimates out to $z \approx 2.5$ (Sulentic et al. 2004, 2006a).

If NLR CIVλ1549 follows [OIII]λ5007 then we expect the strongest and most frequent CIVλ1549 NLR to affect Pop. B sources. Uncorrected CIVλ1549 profiles in Pop. B sources will then be measured with systematically narrow FWHM CIVλ1549. Using this measure for $M_{\rm BH}$ estimation will result in systematic under estimation. This explains why many of previous studies found little or no difference in $M_{\rm BH}$ estimates for RQ and RL sources in direct contradiction with derivations based on FWHM H$\beta_{\rm BC}$. The overall tendency will

be to push both ends towards the center thus reducing the dispersion of $M_{\rm BH}$ derived from uncorrected $M_{\rm BH}$ (see also discussion in Baskin & Laor 2005). $M_{\rm BH}$ underestimates for many sources, especially RL which tend to be overluminous in an optically selected sample (e.g. BG92), will yield spuriously high $L_{\rm bol}/L_{\rm Edd}$ values (e. g. Warner et al. 2004) for Pop. B. The insidious effect of uncorrected CIVλ1549 measures is that it will tend to mix sources of very different empirical and physical properties. The correlation between FWHM CIVλ1549 and $L_{\rm bol}/L_{\rm Edd}$ (Warner et al. 2004, Fig. 5) is almost certainly driven by biases resulting from use of uncorrected CIVλ1549 measures.

6. Conclusions

AGN are widely compared and contrasted in two ways: (1) RQ vs. RL and (2) NLSy1 vs. broad-line Seyferts/quasars. We suggest an alternate approach that unites both of these distinctions and that is supported by differences in CIVλ1549 line measures. We find that sources above and below FWHM H$\beta_{\rm BC} \approx 4000$ km s^{-1} show the most significant spectroscopic (and broadband) differences. RL sources lie largely above this limit while NLSy1 lie below it. We find that all or most sources below 4000 km s^{-1} show properties similar to NLSy1s. Figure 2 (upper left panel) in this paper particularly reenforces this similarity by showing that almost all sources with FWHM H$\beta_{\rm BC} \lesssim 4000$ km s^{-1} show a systematic CIVλ1549 blueshift. Our population A-B concept simply reflects a unification where Pop. A sources show NLSy1-like properties and Pop. B sources show RL-like properties.

This paper addresses two thorny problems involving CIVλ1549 measures and their interpretation: (1) when and how to correct CIVλ1549 for NLR contamination and (2) whether CIVλ1549 measures support previous claims, based on optical spectra (and radio loudness), for two Populations (A+B) of broad line AGN. The second result actually clarifies the answer to the first problem. Evidence is now ubiquitous at both high and low redshift for significant CIVλ1549 NLR emission in many sources. If we used [OIII]λ5007 as a line template then we would find fewer CIV$\lambda1549_{\rm NC}$ components and those found would be narrower and weaker (i.e. lower EW). In several cases we find such an [OIII]λ5007-like component but in many sources our inferred CIV$\lambda1549_{\rm NC}$ component is broader and hence stronger. We argue that empirical evidence (e.g., inflections in some sources and broader CIV$\lambda1549_{\rm NC}$ in Type 2 AGN) as well as simple models support our hypothesis that CIV$\lambda1549_{\rm NC}$ is often not "[OIII]λ5007-like."

We argue that correlations found without NLR correction are very often spurious while real correlations (Figs. 2, 3) require NLR correction to be seen clearly. We propose a simple recipe for CIVλ1549 NLR correction. CIVλ1549 proves to be a valuable 4DE1 space

discriminator that provides evidence in support of our two population hypothesis in the sense that the CIVλ1549 blueshift is ubiquitous only in previously defined population A sources. These results have strong implications for any attempt to use CIVλ1549 measures for black hole mass (and $L_{\rm bol}/L_{\rm Edd}$) estimation. We suggest that any use of CIVλ1549 line measures can be facilitated by interpreting them within the 4DE1 + population A-B context.

We thank the referee for thorough readings of the manuscript. DD acknowledges support from grant IN100703 PAPIIT UNAM. This research has made use of the NASA/IPAC Extragalactic Database (NED) which is operated by the Jet Propulsion Laboratory, California Institute of Technology, under contract with the NASA. Funding for the SDSS and SDSS-II has been provided by the Alfred P. Sloan Foundation, the Participating Institutions, the National Science Foundation, the U.S. Department of Energy, the National Aeronautics and Space Administration, the Japanese Monbukagakusho, the Max Planck Society, and the Higher Education Funding Council for England. The SDSS Web Site is http://www.sdss.org/. The SDSS is managed by the Astrophysical Research Consortium for the Participating Institutions. The Participating Institutions are the American Museum of Natural History, Astrophysical Institute Potsdam, University of Basel, University of Cambridge, Case Western Reserve University, University of Chicago, Drexel University, Fermilab, the Institute for Advanced Study, the Japan Participation Group, Johns Hopkins University, the Joint Institute for Nuclear Astrophysics, the Kavli Institute for Particle Astrophysics and Cosmology, the Korean Scientist Group, the Chinese Academy of Sciences (LAMOST), Los Alamos National Laboratory, the Max-Planck-Institute for Astronomy (MPIA), the Max-Planck-Institute for Astrophysics (MPA), New Mexico State University, Ohio State University, University of Pittsburgh, University of Portsmouth, Princeton University, the United States Naval Observatory, and the University of Washington.

A. Notes on Individual Objects

Most sources follow the 4DE1 trends described here and in previous papers. However a few sources appear to be genuinely pathological. We mention a couple of such sources that appear as outliers in 4DE1 space and that are particularly relevant to the discussion involving CIVλ1549 measures.

3C 57 shows $c(\frac{1}{2})$ CIVλ1549 and $R_{\rm FeII}$ parameters typical of a Pop. A (even extreme Pop. A, NLSy1s) source ($c(\frac{1}{2})$ = –1605 km s^{-1}; $R_{\rm FeII}\approx$ 1.25). W(CIVλ1549) and profile shape are also typical of Pop. A (even similar to the ones of I Zw 1. At the same time it is RL, shows no soft X-ray excess and FWHM(H$\beta_{\rm BC}$) $\approx$ 4700 km s^{-1} all consistent with Pop. B.

PG 0026+126 This quasar is moderate RQ Pop. A following the current 4DE1 empiricism because FWHM(H$\beta_{\rm BC}$) $\approx$ 2400 km s^{-1} and $R_{\rm FeII}\approx$ 0.28. There are two possible interpretations of the CIVλ1549 profile: (1) (FWHM CIVλ1549$\approx$ 1860 km s^{-1} and $c(\frac{1}{2})$ = +140 km s^{-1}) if the strong narrow peak is *not* subtracted or 2)(FWHM CIVλ1549$\approx$ 7000 km s^{-1} and $c(\frac{1}{2})$ $\sim$-1000 km s^{-1}) if the narrow peak is subtracted as a NLR component. This last approach seems especially appropriate since FWHM of the CIVλ1549 narrow core only slightly exceeds (10–20 %) FWHM([OIII]λ5007). The source is a FWHM CIVλ1549 "outlier" whichever CIVλ1549 measure is adopted –either unusually narrow or unusually broad (see Figure 3). $R_{\rm FeII}$ and $\Gamma_{\rm soft}$ measures are intermediate for the source and therefore unconstraining. Note that an erroneous rest frame is often assumed for this source (Gelderman & Whittle 1994). The most accurate redshift for the source corresponds to the centroid of the narrow component which is consistent with the NLR interpretation. This also yields a modest blueshift for the broader component which is also unconstraining. The strong profile inflection and small FWHM for the unshifted narrow component lead us to subtract it as NLR emission. RQ sources like NGC 4253 and 4395 show similar NLR-strong profiles.

PKS 1252+119 Is the highest-z quasar in our sample. Hβ is consequently located at the edge of an excellent SDSS spectrum, making measures of FWHM(H$\beta_{\rm BC}$) uncertain. The reported $R_{\rm FeII}$ is the only upper limit in our sample (marked with an arrow in Fig. 2). This source maybe located in an area of the 4DE1 optical plane where other core-dominated RL sources are found (Fig. 1 of Sulentic et al. 2003) but confirmatory optical data are needed.

REFERENCES

Allen, D. A., Norris, R. P., Meadows, V. S., & Roche, P. F. 1991, MNRAS, 248, 528

Aoki, K., Kawaguchi, T., & Ohta, K. 2005, ApJ, 618, 601

Bachev, R., Marziani, P., Sulentic J. W., Dultzin-Hacyan D., Calvani M. 2004, ApJ, 617, 171

Baldwin, J., Ferland, G., Korista, K., & Verner, D. 1995, ApJ, 455, L119

Barger, A. J., Cowie, L. L., Brandt, W. N., Capak, P., Garmire, G. P., Hornschemeier, A. E., Steffen, A. T., & Wehner, E. H. 2002, AJ, 124, 1839

Baskin, A. & Laor, A. 2004, MNRAS, 350, 31

Baskin, A. & Laor, A. 2005, MNRAS, 356, 1029

Boller, T. 2004, Progress of Theoretical Physics Supplement, 155, 217

Boroson, T.A. 2002, ApJ, 565, 78

Boroson, T. 2005, AJ, 130, 381

Boroson, T. A., & Green, R. F. 1992, ApJS, 80, 109

Bottorff, M. et al. 1997, ApJ, 479, 200

Brotherton, M. S. 1996, ApJS, 102, 1

Brotherton, M. S., & Francis, P. J. 1999, ASP Conf. Ser. 162: Quasars and Cosmology, 162, 395

Brotherton, M. S., Wills, B. J., Francis, P. J., & Steidel, C. C. 1994, ApJ, 430, 495

Chaffee, F. H., Foltz, C. B., Hewett, P. C., Francis, P. A., Weymann, R. J., Morris, S. L., Anderson, S. F., & MacAlpine, G. M. 1991, AJ, 102, 461

Cirasuolo, M., Celotti, A., Magliocchetti, M., & Danese, L. 2003, MNRAS, 346, 447

Collin, S., Kawaguchi, T., Peterson, B. M., & Vestergaard, M. 2006, A&A, 456, 75

Contini, M., & Viegas, S. M. 2001, ApJS, 132, 211

Corbin, M. R. 1991, ApJ, 371, L51

Corbin, M. R. 1997, ApJS, 113, 245

Corbin, M. & Boroson, T. 1996, ApJS, 107, 69

Dawson, S., Stern, D., Bunker, A. J., Spinrad, H., & Dey, A. 2001, AJ, 122, 598

Eracleous, M., & Halpern, J. P. 2004, ApJS, 150, 181

Foltz, C. B., Chaffee, F. H., Hewett, P. C., Weymann, R. J., Anderson, S. F., & MacAlpine, G. M. 1989, AJ, 98, 1959

Gelderman, R. & Whittle, M. 1994, ApJS, 91, 491

Giveon, U., Maoz, D., Kaspi, S., Netzer, H., & Smith, P. S. 1999, MNRAS, 306, 637

Grupe, D., Beuermann, K., Mannheim, K., & Thomas, H.-C. 1999, A&A, 350, 805

Grupe, D., Thomas, H.-C., & Beuermann, K. 2001, AAp, 367, 470

Hewitt, A., & Burbidge, G. 1980, ApJS, 43, 57

Hewitt, A., & Burbidge, G. 1989, A new optical catalog of QSO (1989), 0

Jackson, N., & Browne, I. W. A. 1991, MNRAS, 250, 414

Jarvis, M. J., van Breukelen, C., & Wilman, R. J. 2005, MNRAS, 358, L11

Jiang, L., Fan, X., Ivezic, Z., Richards, G. T., Schneider, D. P., Strauss, M. A., & Kelly, B. C. 2006, ArXiv Astrophysics e-prints, arXiv:astro-ph/0611453

Kaspi S., Smith P.S., Netzer H., et al. 2000, ApJ, 533, 631

Keel, W. C. 1996, ApJS, 106, 27

Kraemer, S. B., Crenshaw, D. M., Filippenko, A. V., & Peterson, B. M. 1998, ApJ, 499, 719

Kraemer, S. B., Wu, C.-C., Crenshaw, D. M., & Harrington, J. P. 1994, ApJ, 435, 171

Kuraszkiewicz, J.K. et al. 2002, ApJS, 143, 257

Kuraszkiewicz, J.K. et al. 2004, ApJ, 150, 165

Laor, A., & Brandt, W. N. 2002, ApJ, 569, 641

Lynds, C. R. 1967, ApJ, 147, 837

Maccarone, T. et al. 2005, A&A, 433, 53

Meiksin, A. 2006, MNRAS, 365, 833

Mainieri, V. et al. 2005, MNRAS, 356, 1571

Marziani P., Sulentic J.W., Dultzin-Hacyan D., Calvani M., Moles M., 1996, ApJS 104, 37

Marziani P., Sulentic J.W., Zwitter T., Dultzin-Hacyan D., Calvani M., 2001, ApJ, 558, 553 (M01)

Marziani P., Sulentic J. W., Zamanov R., Calvani M., Dultzin-Hacyan D., Bachev R., Zwitter T., 2003a, ApJS, 145, 199 (M03)

Marziani P., Zamanov R., Sulentic J. W., Calvani M., 2003b, MNRAS, 345, 1133

Marziani P., Dultzin-Hacyan D., & Sulentic J.W.2006, in: New Developments in Black Hole Research, Editor: Paul V. Kreitler, Nova Science Publishers, p. 123

Murray, N., Chiang, J., Grossman, S. A., & Voit, G. M. 1995, ApJ, 451, 498

Norman, C., et al. 2002, ApJ, 571, 218

Osterbrock, D. E., & Pogge, R. W. 1985, ApJ, 297, 166

Peterson, B. M., et al. 2004, ApJ, 613, 682

Proga, D. & Kallman, T.R. 2004, ApJ, 616, 688

Reichard, T. A., et al. 2003, AJ, 126, 2594

Richards, G. T., Vanden Berk, D. E., Reichard, T. A., Hall, P. B., Schneider, D. P., SubbaRao, M., Thakar, A. R., & York, D. G. 2002, AJ, 124, 1

Rodríguez-Pascual, P.M., Mas-Hesse, J.M., Santos-Lleo, M., 1997, AAp, 327, 72

Schlegel, D. J., Finkbeiner, D. P., & Davis, M. 1998, ApJ, 500, 525

Savage, B. D., et al. 2000, ApJS, 129, 563

Severgnini, P., et al. 2006, A&A, 451, 859

Stern, D., et al. 2002, ApJ, 568, 71

Sulentic, J.W. & Marziani, P., 1999, ApJ, 518, L9

Sulentic, J.W. et al. 2000a, AR A&A, 38, 521 (S00a)

Sulentic, J.W. et al. 2000b, ApJ, 536, L5 (S00b)

Sulentic, J. W., Marziani, P., Zwitter, T., Dultzin-Hacyan, D., & Calvani, M. 2000c, ApJL, 545, L15

Sulentic, J. W., Marziani, P., Zamanov, R., Bachev, R., Calvani, M., & Dultzin-Hacyan, D. 2002, ApJ, 566, L71

Sulentic, J.W. et al. 2003, ApJ, 597, L17

Sulentic, J.W. et al. 2004, A&A, 423, 121

Sulentic, J. W., Dultzin-Hacyan, D.., Marziani, P., Bongardo, C., Braito V., Zamanov, R., Calvani, M. 2006, RevMexAAp, 42, 23

Sulentic, J. W., Repetto, P., Stirpe, G. M., Marziani, P., Dultzin-Hacyan, D., & Calvani, M. 2006, A&A, 456, 929

Szokoly, G. P., et al. 2004, ApJS, 155, 271

Tadhunter, C. N., Morganti, R., di Serego-Alighieri, S., Fosbury, R. A. E., & Danziger, I. J. 1993, MNRAS, 263, 999

Turler, M., & Courvoisier, T. J.-L. 1998, A&A, 329, 863

Turner, T.J., George, I.M., Nandra, K., & Turcan, D., 1999, ApJ, 524, 667

Véron-Cetty, M.-P., Véron, P., & Gonçalves, A. C. 2001, AAp, 372, 730

Vestergaard, M. 2002, ApJ, 571, 733

Vestergaard, M., & Peterson, B. M. 2006, ApJ, 641, 689

Wang, T. et al. 1996, A&A, 309, 81

Warner, C. et al. 2004, ApJ, 608, 136

Wills, D., & Lynds, R. 1978, ApJS, 36, 317

Wills, B. J., et al. 1993, ApJ, 415, 563

Wills, B. J., Laor, A., Brotherton, M. S., Wills, D., Wilkes, B. J., Ferland, G. J., & Shang, Z. 1999, ApJ, 515, L53

Wills, B. J., et al. 1995, ApJ, 447, 139

Wisotzki, L., Christlieb, N., Bade, N., Beckmann, V., Köhler, T., Vanelle, C., & Reimers, D. 2000, A&A, 358, 77

Yuan, M. J. & Wills, B. J. 2003, ApJL, 593, L11

Zamanov, R., Marziani, P., Sulentic, J. W., Calvani, M., Dultzin-Hacyan, D., & Bachev, R. 2002, ApJL, 576, L9

Table 1. Source Identification and 4DE1 Parameters

IAU Code	Common Name[a]	z[b]	z Ref.	PG/BO	A_B[c] [mag]	FWHM(Hβ_{BC}) [km s^{-1}]	R_{FeII}	log(R_K)	Γ_{soft}
(1)	(2)	(3)	(4)	(5)	(6)	(7)	(8)	(9)	(10)
J00057+0203	LBQS 0003+0146	0.234	C91		0.10	3315	0.26	-1.00	3.08
J00059+1609	PG 0003+158	0.4504	M03	*	0.22	5519	0.14	2.53	2.34
J00063+2012	MRK 0335	0.0252	M03	*	0.15	1950	0.28	-0.54	2.90
J00204+0226	LBQS 0017+0209	0.401	F89		0.10	2535	1.07	-1.00	...
J00292+1316	PG 0026+129	0.1451	M03	*	0.31	2405	0.28	-0.10	2.07
J00392−5117	[WPV85] 007	0.0290	G99		0.05	1203	0.68	...	9.00:
J00449+1026	[HB89] 0042+101	0.5857	SPM		0.29	8978	0.40	0.00	2.48
J00470+0319	PG 0044+030	0.6231	M03		0.09	5759	0.19	1.83	1.72
J00535+1241	UGC 00545	0.0605	M03	*	0.28	1151	1.30	-0.47	3.10
J00548+2525	PG 0052+251	0.1543	M03	B*	0.21	5772	0.15	-0.39	2.49
J00573−2222	TON S180	0.0620	M03		0.06	1131	0.54	-1.00	2.89
J01032+0221	LBQS 0100+0205	0.394	M03		0.09	6682	0.20	-1.00	...
J01237−5848	Fairall 9	0.0461	M03		0.12	6263	0.43	-0.30	2.42
J01342−4258	HE 0132−4313	0.237	W00		0.07	2600	2.20	1.57	3.30
J01376−2430	[HB89] 0135−247	0.835	JB91		0.05	10563	0.30	3.59	2.14
J01399+0131	UM 355	0.2600	SPM?		0.13	11245	0.09	3.09	1.93
J02019−1132	3C 057	0.6713	SPM		0.10	4753	1.25	2.00	2.28
J02171+1104	[HB89] 0214+108	0.408	HB80		0.47	4290	0.05	2.68	2.13
J03198+4130	NGC 1275	0.0175	M96		0.70	5659	0.05	3.56	2.40
J03514−1429	3C 095	0.616	M03		0.34	9516	0.22	2.79	2.34
J04055−1308	[HB89] 0403−132	0.5705	M03		0.25	4440	0.07	3.74	1.60
J04172−0553	3C 110	0.7744	SPM		0.19	9256	0.55	2.32	2.48
J04200−5456	NGC 1566	0.00507	ESO		0.04	5967	0.05	2.37	2.19
J04232−0120	[HB89] 0420−014	0.915	WL78		0.57	3185	0.02	3.44	2.02
J04412−4313	[HB89] 0439−433	0.5938	M03		0.07	3608	0.16	2.46	2.25
J04525−2953	IRAS 04505−2958	0.2855	ESO		0.06	2275	0.39	-1.00	3.10
J04561−2159	[HB89] 0454−220	0.5346	SPM		0.18	9042	0.18	2.76	1.97
J05161−0008	ARK 120	0.0323	M03		0.55	6455	0.51	-0.52	2.60
J05198−4546	PICTOR A	0.0350	EH04		0.19	18400	0.01	2.00	2.34
J06300+6905	HS 0624+6907	0.3702	M03		0.42	3660	0.14	-1.00	3.80
J06357−7516	[HB89] 0637−752	0.651	T93		0.42	7922	0.40	3.53	2.38
J07086−4933	1H 0707−495	0.0408	ESO		0.41	1365	1.43	-1.00	2.25
J07456+3142	FBQS J074541.6+314256	0.4611	M03		0.31	7800	0.09	2.66	1.56
J08407+1312	3C 207	0.6804	M03		0.40	2958	0.73	3.79	1.55
J08535+4349	[HB89] 0850+440	0.5149	M03		0.15	2724	0.23	-1.00	...
J09065+1646	3C 215	0.4113	SPM		0.17	4680	0.03	3.32	1.72
J09199+5106	NGC 2841 UB3	0.5563	M96	B	0.07	6338	0.70	-1.00	2.41
J09270+3902	[HB89] 0923+392	0.6953	SDSS		0.06	12675	0.05	4.46	2.25
J09508+3926	PG 0947+396	0.2067	M03	*	0.08	5389	0.26	-1.00	2.18
J09568+4115	PG 0953+414	0.2347	M03	*	0.05	3413	0.22	-0.13	2.65
J09583+3224	3C 232	0.5298	M03		0.06	13666	0.138	3.40	1.46
J10040+2855	PG 1001+291	0.3298	M03	B	0.09	1853	0.92	-1.00	4.01
J10043+0513	PG 1001+054	0.1611	M03	*	0.07	1879	0.49	-0.07	4.38
J10104+4132	FBQS J101027.5+413238	0.6126	M03		0.06	2964	0.22	2.76	2.00

Table 1—Continued

IAU Code	Common Name[a]	z[b]	z Ref.	PG/BO	A_B[c] [mag]	FWHM($H\beta_{BC}$) [km s^{-1}]	R_{FeII}	$\log(R_K)$	Γ_{soft}
(1)	(2)	(3)	(4)	(5)	(6)	(7)	(8)	(9)	(10)
J10235+1951	NGC 3227	0.0039	O03		0.10	4605	0.01	0.00	1.20
J10309+3102	FBQS J103059.1+310255	0.1780	SPM		0.09	7800	0.02	2.38	2.26
J10518−0051	PG 1049−005	0.3591	M03	∗	0.25	5610	0.15	-1.00	2.86
J10525+6125	[HB89] 1049+616	0.4207	SDSS		0.06	4225	0.03	2.61	2.26
J11042+7658	PG 1100+772	0.3116	M03	∗	0.15	8242	0.01	2.62	2.56
J11067+7234	NGC 3516	0.0088	K96		0.18	6338	0.36	0.00	2.20
J11072+1628	[HB89] 1104+167	0.632	C93		0.08	7150	0.02	2.47	2.39
J11146+4037	3C 254	0.7367	SDSS		0.06	6866	0.20	2.00	2.39
J11171+4413	PG 1114+445	0.1433	M03	∗	0.07	5402	0.10	-1.00	2.50
J11185+4025	PG 1115+407	0.1536	M03	∗	0.07	2295	0.49	-1.00	2.92
J11191+2119	PG 1116+215	0.1765	M03	∗	0.10	3218	0.36	-0.20	2.60
J11246+4201	PG 1121+422	0.2253	M03	∗	0.10	2834	0.23	-1.00	2.83
J11350−0318	LBQS 1132−0302	0.236	W00		0.17	2600	1.30	-1.00	...
J11390−3744	NGC 3783	0.0095	M03		0.51	3757	0.18	0.02	2.50
J11391−1350	[HB89] 1136−135	0.5562	SPM		0.17	4584	0.10	3.19	1.78
J11399+6547	3C 263	0.6465	M03		0.05	5012	0.85	3.02	2.12
J11413+0148	LBQS 1138+0204	0.3821	SDSS		0.10	4225	0.92	-1.00	...
J11473−0132	LBQS 1144−0115	0.3827	SDSS	B	0.08	4753	0.43	0.00	...
J11534+4931	SBS 1150+497	0.3336	M03		0.09	4303	0.20	3.13	1.99
J11586+6254	[HB89] 1156+631	0.5924	SDSS		0.07	17956	0.00	0.00	2.30
J11594+2106	[HB89] 1156+213	0.349	HB89		0.12	13000	0.17	2.13	...
J12047+2754	GQ Com	0.1654	M03	∗	0.09	5194	0.10	-0.32	2.24
J12142+1403	PG 1211+143	0.0811	M03	∗	0.15	1989	0.47	-0.89	1.88
J12184+2948	NGC 4253	0.0124	M03		0.08	2087	1.14	0.04	2.50
J12193+0638	PG 1216+069	0.3322	M03	∗	0.09	7072	0.17	0.30	2.38
J12217+7518	MRK 0205	0.0711	M03		0.18	3783	0.21	-0.47	2.10
J12258+3332	NGC 4395	0.0008	M03		0.07	1695	0.47	-2.45	1.2
J12291+0203	3C 273	0.1583	M03	∗	0.09	3829	0.30	2.11	2.11
J12334+0931	LBQS 1230+0947	0.4159	SDSS		0.09	4225	0.03	-1.00	3.79
J12524+5634	SBS 1250+568	0.3200	SDSS		0.05	4810	0.01	3.52	2.59
J12546+1141	[HB89] 1252+119	0.8737	SDSS		0.19	3600:	$\lesssim 0.9$	2.95	1.88
J13012+5902	SBS 1259+593	0.4776	M03	∗	0.03	3569	1.07	-1.00	...
J13055−1033	PG 1302−102	0.2783	M03	∗	0.18	3959	0.64	2.42	2.31
J13079+0642	3C 281	0.599	B96		0.17	8915	0.01	2.00	2.03
J13097+0819	PG 1307+085	0.1546	M03	∗	0.15	5616	0.10	-1.00	2.58
J13122+3515	FBQS J131217.7+351521	0.1821	M03	∗	0.05	4186	0.19	1.33	2.51
J13198−0158	LBQS 1317−0142	0.225	W00		0.11	2275	0.87	-1.00	...
J13238+6541	PG 1322+659	0.1674	M03	∗	0.08	3114	0.34	-1.00	3.00
J13253−3824	2MASX J13251937-382452	0.0667	A91		0.30	1246	0.48	0.00	4.40
J13532+6345	PG 1351+640	0.0882	M03	∗	0.09	5876	0.12	0.66	2.43
J13545+1805	PG 1352+183	0.1508	M03	∗	0.08	4947	0.44	-1.00	2.65
J13570+1919	[HB89] 1354+195	0.7197	M03		0.26	4960	0.06	3.27	0.88
J13590−4152	[HB89] 1355−416	0.3145	T93		0.37	8978	0.10	2.94	1.96
J14052+2555	FBQS J140516.1+255534	0.1633	M03	B∗	0.07	2041	0.84	-0.35	2.90

Table 1—Continued

IAU Code	Common Name[a]	z[b]	z Ref.	PG/BO	A_B[c] [mag]	FWHM(Hβ_{BC}) [km s^{-1}]	R_{FeII}	log(R_K)	Γ_{soft}
(1)	(2)	(3)	(4)	(5)	(6)	(7)	(8)	(9)	(10)
J14063+2223	PG 1404+226	0.0973	M03	∗	0.10	956	0.93	-0.23	3.07
J14170+4456	PG 1415+451	0.1151	M03	B∗	0.04	2691	1.03	-1.00	3.30
J14179+2508	NGC 5548	0.0168	M03		0.09	6143	0.33	0.11	2.30
J14190−1310	[HB89] 1416−129	0.1294	M03	∗	0.40	6617	0.10	0.48	2.09
J14274+1949	MRK 0813	0.1105	SPM		0.14	9612	0.30	-1.00	2.64
J14275+2632	[HB89] 1425+267	0.3634	M03	∗	0.08	9224	0.08	1.83	2.10
J14297+4747	[HB89] 1427+480	0.2199	M03	∗	0.07	2782	0.26	-1.00	2.47
J14421+3526	MRK 0478	0.0771	M03	∗	0.06	1794	0.93	-0.73	2.91
J14467+4035	[HB89] 1444+407	0.2670	M03	∗	0.06	3101	1.20	-1.00	2.99
J14544−3747	[HB89] 1451−375	0.314	C97		0.34	4869	0.17	2.00	2.43
J15147+3650	[HB89] 1512+370	0.3710	M03	∗	0.09	10485	0.15	2.68	2.21
J15395+4735	[HB89] 1538+477	0.7723	M03	∗	0.07	5857	0.34	1.18	1.96
J15455+4846	[HB89] 1543+489	0.3978	M03	B∗	0.08	1638	0.64	0.10	3.11
J15477+2052	PG 1545+210	0.2659	M03	∗	0.18	7670	0.11	3.08	2.43
J15591+3501	UGC 10120	0.0313	SPM		0.11	800	1.16	-0.54	3.05
J16142+2604	[HB89] 1612+261	0.1308	M03	∗	0.23	2542	0.10	0.30	2.26
J16203+1736	3C 334	0.5556	M03		0.18	11219	0.09	2.76	2.10
J16246+2345	3C 336	0.927	B96		0.31	7499	0.01	2.00	...
J16279+5522	SBS 1626+554	0.1326	M03	∗	0.03	4888	0.31	-1.00	2.61
J16303+3756	[HB89] 1628+380	0.3945	SPM		0.04	7394	0.15	0.00	1.65
J16429+3948	3C 345	0.5931	M03		0.06	4498	0.30	3.57	1.81
J17046+6044	SBS 1704+608	0.372	M03	∗	0.10	9224	0.11	2.64	2.31
J18219+6420	[HB89] 1821+643	0.2972	M03		0.18	6968	0.25	0.98	2.42
J18421+7946	3C 390.3	0.0555	M03		0.31	12688	0.12	3.24	1.80
J19278+7358	[HB89] 1928+738	0.3021	M03		0.57	3582	0.19	3.39	1.80
J20441−1043	MRK 0509	0.0344	M03		0.25	3614	0.04	-0.61	2.61
J21148+0607	[HB89] 2112+059	0.4608	M03	∗	0.39	4173	0.53	-0.25	1.85
J21315−1207	[HB89] 2128−123	0.4996	M03		0.27	6468	0.01	3.18	1.86
J21377−1432	[HB89] 2135−147	0.2004	M03		0.22	9789	0.11	2.77	2.32
J21435+1743	[HB89] 2141+175	0.2106	M03		0.48	5298	0.33	2.73	2.44
J22032+3145	[HB89] 2201+315	0.2952	M03		0.53	3497	0.81	3.12	2.20
J22188−0335	[HB89] 2216−038	0.901	L67		0.41	3900	0.39	3.20	2.64
J22426+2943	UGC 12163	0.0245	M03		0.26	1300	0.87	0.34	3.40
J22463−1206	[HB89] 2243−123	0.6255	M03		0.22	4472	0.14	3.44	3.50
J22539+1608	3C 454.3	0.8586	KPNO		0.46	7394	0.10	1.36	1.59
J22540−1734	MR 2251−178	0.0638	M03		0.17	7176	0.09	-0.34	2.39
J22541+1136	[HB89] 2251+113	0.3256	M03	∗	0.37	4752	0.24	2.52	...
J23032+0852	NGC 7469	0.0160	M03		0.30	2789	0.01	0.44	2.40
J23037−6807	[HB89] 2300−683	0.5158	M03		0.13	7625	0.16	2.52	2.65
J23112+1008	[HB89] 2308+098	0.4341	M03	∗	0.18	9373	0.08	2.24	2.34
J23466+0930	[HB89] 2344+092	0.6719	M03		0.31	3159	0.20	2.97	2.34
J23519−0109	[HB89] 2349−014	0.1740	M03		0.12	5805	0.20	2.42	2.44

Note. — Table 1 is published in its entirety in the electronic edition of the Astrophysical Journal. A portion is shown here for guidance regarding its form and content.

[a]In a format recognized by NED.

[b]Accuracy of z values can be in general assumed to be ± 0.0001 at a 1–σ confidence level in case four decimal digits are provided; ± 0.001 otherwise.

[c]From Schlegel et al. (1998)

References. — M03: (Marziani et al. 2003a); G99: Grupe et al. (1999) SDSS: Spectra retrieved from www.sdss.org. z values were measured as described in the text of the paper, and may differ from those reported in NED. L67: Lynds (1967). SPM: Unpublished spectra obtained with the 2.2m telescope at San Pedro Martir. B96: Brotherton (1996). ESO: Unpublished ESO spectra. KPNO: unpublished KPNO spectra. T93: Tadhunter et al. (1993). JB91: Jackson & Browne (1991) C97: Corbin (1997). M96: Marziani et al. (1996). LBQS: W00: Wisotzki et al. (2000) A91: K96: Keel (1996). EH04: Eracleous & Halpern (2004). A91: Allen et al. (1991). HB89: Hewitt & Burbidge (1989). HB80: (Hewitt & Burbidge 1980).

Table 2. CIVλ1549 Emission Line Parameters

IAU Code (1)	f_λ[a] (2)	F_{NC}[b] (3)	Δv_{rNC}[d] (4)	F_{BC}[c] (5)	$c(\frac{1}{4})$[d] (6)	Δ^- [d] (7)	Δ^+ [d] (8)	$c(\frac{1}{2})$[d] (9)	Δ^{-d} (10)	Δ^{+d} (11)	$c(3/4)$ (12)	Δ^d (13)	c(0.9)[d] (14)	Δ^d (15)	FWHM[d] (16)	Δ^d (17)	A.I. (18)	Δ^- (19)	Δ^+ (20)	$Kurt.$ (21)	Δ (22)
00057+0203	0.55	0.23	-726	4.0	-824	331	560	-455	121	120	-404	110	-365	78	4168	252	-0.12	0.10	0.16 0.16	0.35	0.06
00059+1609	2.53	1.94	-66	22.5	866	591	522	35	200	228	-8	143	-1	92	5347	455	0.16	0.12	0.10 0.12	0.29	0.04
00063+2012	7.97	7.33	314	50.7	-221	259	229	19	98	94	147	81	195	53	2927	195	-0.17	0.11	0.10 0.11	0.37	0.05
00204+0226	0.44	0.00	···	1.2	-2426	174	155	-2144	122	117	-2063	140	-2064	106	5378	244	-0.10	0.07	0.07 0.07	0.50	0.05
00292+1316	2.82	1.64	95	8.5	1035	1077	244	-501	199	215	-201	261	-19	160	8595	429	0.14	0.17	0.06 0.17	0.36	0.06
00392-5117	0.20	A	···	2.0	338	262	265	-78	108	186	-54	81	-6	55	3056	371	0.11	0.09	0.09 0.09	0.28	0.03
00449+1026	0.12	0.18	56	2.3	1433	846	705	-37	268	281	-124	203	-144	125	7385	563	0.20	0.10	0.09 0.10	0.26	0.04
00470+0319	1.09	0.22	126	8.2	-418	322	490	-750	203	229	-568	143	-591	91	6274	458	0.03	0.07	0.10 0.10	0.33	0.04
00535+1241	3.25	A	···	8.7	-2264	338	212	-1669	110	211	-875	68	-954	47	3804	422	-0.47	0.07	0.06 0.07	0.27	0.04
00548+2525	2.11	0.74	-378	27.7	-104	767	649	-800	292	289	-624	177	-604	107	6659	585	0.08	0.12	0.10 0.12	0.28	0.04
00573-2222	4.01	1.32	-273	13.8	-1232	386	245	-801	165	154	-588	108	-563	67	3973	330	-0.21	0.11	0.08 0.11	0.35	0.05
01032+0221	0.43	0.00	···	4.7	-60	867	556	-427	185	225	-356	126	-297	77	4598	450	0.05	0.19	0.12 0.19	0.27	0.06
J01237-5848	2.41	3.68	-6	41.1	21	375	441	234	128	131	157	107	106	76	4100	261	-0.02	0.10	0.11 0.11	0.31	0.04
01342-4258	1.68	0.00	···	1.0	-3333	164	170	-2665	173	166	-2195	146	-2026	99	5233	346	-0.36	0.06	0.06 0.06	0.45	0.04
01376-2430	0.87	A	···	3.9	917	518	528	194	240	234	-85	147	-176	92	5663	481	0.23	0.09	0.10 0.10	0.32	0.05
01399+0131	0.13	0.00	···	3.3	1261	621	672	1930	471	262	214	133	269	79	8327	941	0.15	0.11	0.12 0.12	0.20	0.03
02019-1132	2.64	0.00	···	4.8	-1686	258	512	-1531	156	156	-1267	167	-1088	116	5971	312	-0.14	0.08	0.14 0.14	0.45	0.07
02171+1104	1.30	0.71	-131	19.8	-6	937	853	-214	217	204	-97	142	-66	92	5296	434	0.01	0.15	0.14 0.15	0.24	0.04
03198+4130	0.29	0.00	···	1.4	-122	74	83	-190	61	63	-198	69	-190	50	2557	125	0.04	0.07	0.07 0.07	0.48	0.05
03514-1429	3.94	0.86	-12	20.2	0	1362	1940	-78	382	322	194	247	277	172	9649	763	-0.03	0.15	0.21 0.21	0.31	0.07
04055-1308	0.65	0.49	294	4.1	697	433	513	560	180	187	514	139	522	98	5398	375	0.03	0.09	0.11 0.11	0.33	0.04
04172-0553	2.02	1.11	-134	16.2	1586	612	507	983	301	336	582	247	386	163	9018	672	0.16	0.09	0.08 0.09	0.36	0.04
04200-5456	0.18	0.42	443	1.9	1117	218	239	993	107	108	910	99	874	66	3602	216	0.09	0.09	0.09 0.09	0.40	0.05
04232-0120	0.48	0.13	-285	4.2	-3	370	630	181	133	127	68	119	-25	70	4021	267	0.01	0.11	0.18 0.18	0.33	$^{+0.05}_{-0.37}$
04412-4313	0.83	0.59	-54	6.5	-577	339	547	-7	127	119	-53	110	-103	76	4079	254	-0.12	0.09	0.15 0.15	0.33	0.05
04525-2953	1.41	0.00	···	8.5	-1579	222	279	-898	131	115	-820	108	-818	79	4168	261	-0.21	0.07	0.08 0.08	0.38	0.04
04561-2159	1.99	0.82	-302	17.3	2460	946	2099	110	329	462	-222	162	-276	108	6520	925	0.31	0.10	0.20 0.20	0.21	0.05
05161-0008	9.86	8.65	-143	126.9	-566	542	447	-236	164	172	-330	126	-307	83	4792	343	-0.06	0.13	0.11 0.13	0.33	0.05
05198-4546	0.18	0.33	51	3.2	975	1785	274	-1111	525	1153	-278	207	-291	124	10017	2306	0.13	0.17	0.04 0.17	0.22	0.05
06300+6905	5.95	0.00	···	5.5	-1428	266	257	-937	168	123	-777	97	-731	67	3666	337	-0.22	0.09	0.10 0.10	0.35	0.05
06357-7516	2.42	1.12	292	14.2	1716	791	768	534	103	110	362	94	285	62	3368	220	0.41	0.15	0.14 0.15	0.29	0.07
07086-4933	2.69	0.00	···	2.3	-2513	583	270	-2032	231	295	-1530	101	-1396	95	4841	589	-0.32	0.13	0.10 0.13	0.42	0.08
07456+3142	1.28	0.93	-308	13.5	409	484	475	258	301	297	-410	238	-679	125	7690	603	0.17	0.09	0.09 0.09	0.33	0.05
08407+1312	0.35	A	···	4.1	890	427	427	425	135	143	319	122	284	83	4570	287	0.16	0.12	0.11 0.12	0.37	0.06
08535+4349	0.79	0.00	···	4.1	-1641	290	282	-1345	215	229	-882	154	-789	87	5448	457	-0.20	0.08	0.08 0.08	0.34	0.04
09065+1646	0.15	0.25	-508	4.0	1972	823	1664	28	186	169	100	153	11	147	7460	372	0.25	0.09	0.17 0.17	0.34	0.07
09199+5106	1.46	0.00	···	4.3	-2301	274	399	-1931	187	181	-1632	164	-1503	110	5998	373	-0.18	0.08	0.11 0.11	0.41	0.05
09270+3902	1.13	0.20	890	8.2	2341	920	477	1240	162	177	1118	140	1082	95	5271	353	0.24	0.20	0.09 0.20	0.31	0.06
09508+3926	1.61	0.50	-284	11.3	73	896	575	-606	128	132	-655	120	-671	84	4532	263	0.18	0.22	0.13 0.22	0.35	0.07
09568+4115	2.39	1.30	-365	15.3	-133	649	684	-286	128	130	-414	117	-487	79	4290	259	0.09	0.16	0.17 0.17	0.32	0.06
09583+3224	43.40	A	···	132.4	1566	473	379	969	325	278	236	165	144	86	6219	649	0.23	0.08	0.07 0.08	0.24	0.03
10040+2855	2.07	0.00	···	7.9	-1934	256	401	-1319	171	149	-994	172	-699	71	3990	343	-0.33	0.07	0.09 0.09	0.30	0.05
10043+0513	0.60	0.30	-561	4.0	-1815	288	619	-930	128	121	-851	115	-828	80	4320	257	-0.25	0.07	0.13 0.13	0.35	0.06
10104+4132	1.83	0.37	21	17.6	-196	431	802	59	170	159	25	105	13	73	4161	340	-0.05	0.10	0.19 0.19	0.29	0.06
10235+1951	0.08	A	···	1.2	-155	201	195	-195	103	104	-220	101	-232	70	3717	208	0.03	0.09	0.09 0.09	0.42	0.05
10309+3102	1.25	1.03	-85	14.6	-187	623	1382	-140	226	231	-188	152	-236	93	5538	462	0.01	0.12	0.25 0.25	0.28	0.08
10518-0051	1.44	0.36	-208	14.7	68	626	354	-453	130	128	-418	117	-407	85	4563	260	0.11	0.15	0.09 0.15	0.35	0.06
10525+6125	1.17	a	···	7.6	1487	686	569	179	209	239	51	180	-4	125	6790	478	0.24	0.11	0.09 0.11	0.33	0.05
11042+7658	1.32	1.12	-33	17.0	211	495	1220	3	386	355	80	190	42	127	7560	771	0.02	0.08	0.17 0.17	0.31	0.06
11067+7234	3.60	A	···	76.5	-861	442	713	68	416	234	214	145	192	94	5494	832	-0.20	0.09	0.16 0.16	0.30	0.05
11072+1628	2.23	0.92	-333	17.6	761	293	376	399	261	266	-29	177	-208	105	6295	532	0.19	0.07	0.08 0.08	0.34	0.04
11146+4037	0.28	0.25	-598	5.1	312	637	575	166	731	637	-448	212	-366	133	8937	1462	0.09	0.09	0.08 0.09	0.29	0.04
11171+4413	0.56	A	···	4.6	233	377	370	351	119	122	299	104	291	69	3797	244	-0.01	0.10	0.10 0.10	0.29	0.04
11185+4025	1.49	a	···	6.8	-735	431	416	-383	165	131	-297	102	-277	71	3989	331	-0.11	0.12	0.12 0.12	0.31	0.04
11191+2119	5.14	0.93	-379	32.1	-822	337	340	-700	225	183	-651	123	-664	85	4842	451	-0.03	0.08	0.08 0.08	0.32	0.04
11246+4201	1.52	0.25	-166	8.9	-195	342	241	-166	75	78	-225	63	-247	42	2327	156	0.03	0.17	0.13 0.17	0.34	0.07
11350-0318	0.36	0.00	···	1.3	-1498	261	912	-1408	136	137	-1152	128	-1041	78	4378	273	-0.14	0.09	0.31 0.31	0.39	0.11
11390-3744	15.42	17.30	147	140.4	-521	420	426	-200	163	145	-295	110	-369	75	4171	326	-0.04	0.11	0.11 0.11	0.31	0.04
11391-1350	1.17	1.31	139	11.3	1177	594	599	674	176	184	415	158	292	102	5620	368	0.18	0.13	0.12 0.13	0.35	0.06
11399+6547	1.82	0.38	14	14.5	-189	773	513	-210	154	157	-327	135	-376	91	4967	314	0.04	0.20	0.13 0.20	0.36	0.08
11413+0148	0.54	a	···	1.8	-1324	204	443	-536	262	253	-566	138	-538	92	5391	523	-0.15	0.05	0.08 0.08	0.29	0.03
11473-0132	0.08	0.01	371	0.3	35	226	226	-40	225	219	364	153	477	91	5434	450	-0.10	0.06	0.06 0.06	0.33	0.04

Table 2—Continued

IAU Code (1)	f_λ[a] (2)	F_{NC}[b] (3)	Δv_{rNC}[d] (4)	F_{BC}[c] (5)	$c(\frac{1}{4})$[d] (6)	Δ^- [d] (7)	Δ^+ [d] (8)	$c(\frac{1}{2})$[d] (9)	Δ^-[d] (10)	Δ^+[d] (11)	$c(3/4)$ (12)	Δ[d] (13)	c(0.9)[d] (14)	Δ[d] (15)	FWHM[d] (16)	Δ[d] (17)	A.I. (18)	Δ^- (19)	Δ^+ (20)	$Kurt.$ (21)	Δ (22)
1534+4931	0.55	0.18	343	8.5	978	425	389	536	161	170	427	134	424	89	4972	341	0.12	0.10	0.09	0.10	0.34	0.04
1586+6254	4.46	0.45	251	7.7	-607	653	1206	-620	355	388	187	274	323	120	8894	776	-0.11	0.09	0.16	0.16	0.24	0.04
1594+2106	0.60	0.32	-424	8.4	-1627	1198	1035	-614	373	265	-511	147	-502	93	5617	746	-0.15	0.15	0.14	0.15	0.21	0.04
2047+2754	0.32	0.61	-475	9.1	-1323	477	544	-876	111	105	-807	97	-776	71	3782	222	-0.16	0.13	0.17	0.17	0.36	0.07
2142+1403	3.06	2.72	-101	22.8	-249	316	168	-89	84	82	-56	84	-41	59	3108	167	-0.09	0.14	0.09	0.14	0.43	0.07
2184+2948	0.03	0.14	-13	0.1	-887	130	127	-590	132	132	-350	168	-224	131	6402	264	-0.16	0.07	0.07	0.07	0.54	0.05
2193+0638	1.79	1.50	72	16.9	-342	829	638	279	209	198	200	129	172	83	4829	417	-0.09	0.14	0.12	0.14	0.25	0.05
2217+7518	3.61	1.25	69	18.8	-117	250	556	-73	119	136	-150	80	-148	72	4097	271	0.01	0.08	0.16	0.16	0.41	$^{+0.03}_{-0.32}$
2258+3332	0.24	1.25	281	1.8	220	215	220	176	112	114	216	114	260	82	4267	229	-0.01	0.09	0.09	0.09	0.43	0.05
2291+0203	29.17	7.63	-634	103.0	433	630	1394	-552	192	205	-500	141	-473	92	5254	409	0.16	0.11	0.21	0.21	0.27	0.07
2334+0931	1.36	0.00	···	8.6	-161	279	310	96	132	119	110	85	119	60	3349	264	-0.08	0.09	0.10	0.10	0.29	0.04
2524+5634	0.29	0.09	66	3.4	94	270	374	20	131	144	-13	89	-18	62	3525	288	0.03	0.08	0.11	0.11	0.31	0.04
2546+1141	1.17	0.00	···	2.6	-1908	168	197	-1567	157	140	-1465	129	-1439	87	4737	313	-0.13	0.07	0.07	0.07	0.40	0.04
3012+5902	2.40	0.00	···	4.8	-5239	329	358	-4325	314	286	-3795	209	-3648	133	7623	628	-0.27	0.07	0.07	0.07	0.37	0.04
3055-1033	3.87	0.24	-360	8.1	-262	458	323	215	212	173	-71	210	-488	114	5484	423	0.05	0.11	0.08	0.11	0.35	0.06
3079+0642	0.52	0.24	384	5.9	134	794	699	140	459	496	181	200	292	120	7727	991	-0.02	0.11	0.10	0.11	0.27	0.04
3097+0819	1.40	0.30	607	13.6	-8	492	499	312	188	166	434	118	422	76	4413	375	-0.11	0.12	0.14	0.14	0.32	0.06
3122+3515	1.60	A	···	11.0	-1272	404	1325	-358	133	129	-223	124	-142	86	4587	266	-0.24	0.10	0.30	0.30	0.31	0.07
3198-0158	0.26	0.00	···	1.6	-1655	231	200	-1073	137	106	-1037	88	-1061	62	3363	274	-0.20	0.08	0.07	0.08	0.35	0.04
3238+6541	1.20	0.41	-35	7.9	-436	341	259	-310	101	101	-237	98	-185	68	3617	202	-0.09	0.12	0.10	0.12	0.40	0.06
3253-3824	1.18	0.00	···	1.8	-3160	214	215	-2764	185	177	-2512	149	-2442	97	5427	370	-0.18	0.07	0.07	0.07	0.40	0.04
3532+6345	2.32	A	···	15.3	78	265	331	-126	103	107	-175	99	-196	68	3660	214	0.09	0.10	0.12	0.12	0.39	0.06
3545+1805	1.27	0.46	-79	10.2	-773	412	788	-372	249	224	-337	148	-375	86	5435	497	-0.08	0.09	0.18	0.18	0.30	0.06
3570+1919	1.66	2.36	132	13.0	1065	477	516	401	263	287	46	179	-107	117	6697	575	0.19	0.08	0.08	0.08	0.31	0.04
3590-4152	3.49	0.48	-114	25.7	-183	560	481	-1069	293	329	-1168	256	-1268	205	10536	658	0.12	0.08	0.07	0.08	0.39	0.04
4052+2555	2.89	0.00	···	13.0	-675	857	362	-719	220	330	-184	113	-86	71	4650	660	-0.15	0.20	0.11	0.20	0.31	0.07
4063+2223	0.62	a	···	2.5	-1571	331	345	-1537	121	117	-1515	106	-1508	72	3910	242	-0.02	0.10	0.11	0.11	0.34	0.05
4170+4456	1.21	0.00	···	8.3	-1148	290	315	-771	130	121	-644	104	-576	70	3822	259	-0.17	0.09	0.10	0.10	0.35	0.05
4179+2508	3.00	4.75	408	59.2	63	459	479	309	191	183	251	174	182	121	6441	382	-0.02	0.10	0.10	0.10	0.39	0.05
4190-1310	0.57	0.00	···	21.1	-843	786	694	-143	144	147	-195	136	-222	93	4996	294	-0.13	0.15	0.14	0.15	0.33	0.06
4274+1949	1.77	0.37	442	17.6	41	552	673	-217	268	279	208	238	445	138	7983	558	-0.06	0.09	0.11	0.11	0.34	0.05
4275+2632	0.78	a	···	10.9	302	1487	2713	-563	313	333	-865	280	-969	200	10843	666	0.14	0.17	0.26	0.26	0.37	$^{+0.05}_{-0.12}$
4297+4747	1.07	0.22	213	8.1	626	383	315	426	96	98	348	87	298	62	3278	197	0.11	0.14	0.11	0.14	0.36	0.06
4421+3526	4.34	a	···	14.3	-765	210	307	-351	73	70	-324	67	-306	49	2569	145	-0.20	0.09	0.12	0.12	0.36	0.06
4467+4035	2.28	0.10	-982	5.3	-1422	268	297	-1143	155	154	-906	161	-764	113	5881	311	-0.16	0.08	0.09	0.09	0.45	0.05
4544-3747	0.59	0.68	159	12.8	975	382	450	777	168	169	608	131	534	81	4676	337	0.10	0.10	0.11	0.11	0.32	0.05
5147+3650	1.56	1.08	218	14.2	-32	1225	510	-622	333	376	-44	198	-22	120	7656	752	0.00	0.17	0.08	0.17	0.28	0.05
5395+4735	2.42	a	···	15.7	-659	571	437	-402	257	237	-227	159	-183	106	6224	514	-0.09	0.11	0.09	0.11	0.35	0.05
5455+4846	1.46	0.00	···	5.9	-2193	1456	379	-1587	177	159	-1263	126	-1099	118	5946	353	-0.25	0.25	0.10	0.25	0.47	$^{+0.04}_{-0.16}$
5477+2052	0.99	0.80	-371	17.4	-26	836	1373	-78	231	233	-138	179	-161	119	6643	465	0.02	0.13	0.20	0.20	0.29	0.06
5591+3501	0.77	0.00	···	6.9	-26	242	223	32	71	69	44	58	48	39	2159	142	-0.04	0.13	0.12	0.13	0.34	0.06
6142+2604	0.68	0.32	442	13.1	1173	423	574	433	164	182	421	127	452	85	4787	363	0.14	0.09	0.11	0.11	0.27	0.04
6203+1736	1.31	0.37	24	9.9	96	561	667	-67	304	311	-162	184	-186	117	6940	621	0.04	0.08	0.10	0.10	0.28	0.04
6246+2345	0.42	0.59	62	4.6	1554	756	742	638	284	320	303	210	260	141	7988	641	0.17	0.11	0.10	0.11	0.32	0.05
6279+5522	2.06	0.40	-273	15.8	-749	461	569	-299	150	154	-389	119	-447	83	4529	307	-0.06	0.10	0.12	0.12	0.29	0.04
6303+3756	0.04	0.00	···	0.8	2088	368	264	941	226	241	851	226	863	169	8837	481	0.17	0.07	0.06	0.07	0.40	0.04
6429+3948	0.55	0.00	···	5.9	389	195	309	250	112	111	166	111	115	73	3936	224	0.09	0.08	0.11	0.11	0.41	0.06
7046+6044	2.00	A	···	15.7	942	1347	822	-200	242	362	-465	121	-503	76	4697	723	0.21	0.17	0.11	0.17	0.19	0.04
8219+6420	7.81	a	···	82.4	1517	408	452	457	221	279	-34	158	-209	92	5421	559	0.36	0.09	0.08	0.09	0.33	0.05
8421+7946	0.59	0.44	45	7.8	-1055	424	1966	-1285	270	275	-2479	297	-2824	126	8186	549	0.25	0.07	0.23	0.23	0.29	0.08
9278+7358	2.11	0.56	146	17.7	28	440	544	209	140	134	200	113	178	80	4365	279	-0.04	0.11	0.14	0.14	0.33	0.05
20441-1043	8.00	a	···	94.2	-790	339	335	-457	142	134	-379	111	-359	74	4098	285	-0.12	0.10	0.10	0.10	0.35	0.05
21148+0607	1.50	0.00	···	7.8	-2192	245	532	-1498	214	180	-1229	156	-1113	112	5978	428	-0.22	0.07	0.14	0.14	0.39	0.05
21315-1207	2.51	0.53	-203	26.2	808	402	589	524	301	276	81	130	4	98	6185	603	0.14	0.08	0.11	0.11	0.31	0.04
21377-1432	0.74	A	···	13.9	-75	681	643	131	194	184	210	101	225	63	3846	388	-0.07	0.15	0.14	0.15	0.23	0.04
21435+1743	1.49	0.00	···	2.6	267	83	83	309	101	101	350	143	375	117	5670	202	-0.03	0.07	0.07	0.07	0.58	0.05
22032+3145	4.90	0.00	···	24.6	213	1013	499	-180	268	284	-180	144	-121	89	5438	567	0.05	0.16	0.08	0.16	0.23	0.04
22188-0335	0.95	0.15	356	6.1	2413	1118	977	1198	416	454	687	154	597	100	6431	908	0.25	0.12	0.11	0.12	0.24	0.04
22426+2943	1.16	A	···	2.5	5	109	110	-61	55	57	-78	46	-81	30	1664	115	0.06	0.09	0.09	0.09	0.36	0.05
22463-1206	1.54	0.50	312	10.6	740	462	671	451	160	177	330	95	306	59	3584	353	0.11	0.12	0.16	0.16	0.25	0.05
22539+1608	1.60	0.13	-203	5.0	-395	262	467	-295	99	98	-183	92	-128	63	3372	199	-0.10	0.11	0.20	0.20	0.40	0.08
22540-1734	2.50	a	···	70.4	-946	495	1194	-321	161	145	-101	110	-34	71	4044	323	-0.25	0.12	0.39	0.39	0.32	$^{+0.05}_{-0.11}$

Table 2—Continued

IAU Code (1)	f_λ[a] (2)	F_{NC}[b] (3)	Δv_{rNC}[d] (4)	F_{BC}[c] (5)	$c(\frac{1}{4})$[d] (6)	Δ^- [d] (7)	Δ^+ [d] (8)	$c(\frac{1}{2})$[d] (9)	Δ^-[d] (10)	Δ^+[d] (11)	$c(3/4)$ (12)	Δ[d] (13)	c(0.9)[d] (14)	Δ[d] (15)	FWHM[d] (16)	Δ[d] (17)	A.I. (18)	Δ^- (19)	Δ^+ (20)	*Kurt.* (21)	Δ (22)
J22541+1136	1.39	a	···	19.4	-823	702	931	-399	145	141	-257	111	-202	71	4053	290	-0.13	0.16	0.20 0.20	0.26	0.05
J23032+0852	5.12	5.88	141	59.5	-258	371	478	104	155	139	108	121	70	84	4563	310	-0.08	0.10	0.13 0.13	0.34	0.05
J23037-6807	0.63	a	···	12.1	779	520	626	142	145	159	11	107	-27	70	3958	318	0.15	0.10	0.12 0.12	0.22	0.03
J23112+1008	1.32	a	···	12.3	904	872	941	-73	161	162	-200	137	-281	92	5037	324	0.18	0.12	0.13 0.13	0.23	0.04
J23466+0930	1.76	1.08	108	7.2	-362	462	673	-111	116	118	-72	110	-29	78	4132	236	-0.08	0.12	0.17 0.17	0.33	0.06
J23519-0109	0.38	0.32	-633	11.2	-1739	452	680	-1166	245	224	-797	188	-628	130	7050	490	-0.20	0.09	0.14 0.14	0.38	0.06

Note. — Table 2 is published in its entirety in the electronic edition of the Astrophysical Journal. A portion is shown here for guidance regarding its form and content.

[a]Specific continuum flux at 1550 Å in units of ergs s^{-1} $Å^{-1}$ $cm^{-2} \times 10^{14}$.

[b]Flux of CIVλ1549$_{NC}$ in units of ergs s^{-1} $cm^{-2} \times 10^{13}$. The letter "A" indicate major absorptions (typically of mini-BALs) affecting the profile of CIVλ1549$_{BC}$. "a" indicates narrow absorptions that "eat away" CIVλ1549$_{NC}$ but that do not hamper CIVλ1549$_{BC}$ measurements.

[c]Flux of CIVλ1549$_{BC}$ in units of ergs s^{-1} $cm^{-2} \times 10^{13}$.

[d]In units of km s^{-1}.

Table 3. AVERAGE VALUES[a]

AGN pop	$N_{\rm sources}$	EW(CIVλ1549$_{\rm BC}$) [Å]	$c(\frac{1}{2})$ CIVλ1549$_{\rm BC}$ [km s^{-1}]	FWHM(CIVλ1549$_{\rm BC}$) [km s^{-1}]	FWHM(H$\beta_{\rm BC}$) [km s^{-1}]	$R_{\rm FeII}$	$\Gamma_{\rm Soft}$
(1)	(2)	(3)	(4)	(5)	(6)	(7)	(8)
All QSO	130	93 (66)	−294 (837)	5284 (1787)	5387 (3268)	0.36 (0.38)	2.41 (0.58)
RQ only	71	84 (69)	−582 (860)	4733 (1482)	4100 (2681)	0.48 (0.43)	2.64 (0.63)
RL only	59	104 (60)	+52 (667)	5946 (1905)	6936 (3259)	0.22 (0.25)	2.15 (0.38)
Pop. A	52	57 (34)	−677 (966)	4451 (1269)	2604 (891)	0.60 (0.45)	2.67 (0.68)
Pop. B	78	117 (71)	−39 (627)	5839 (1871)	7242 (2943)	0.20 (0.22)	2.24 (0.43)

[a]The number in parenthesis indicates the sample standard deviation.

Table 4. CORRELATION ANALYSIS FOR CIVλ1549$_{BC}$ PARAMETERS[a]

CIVλ1549$_{BC}$	W		FWHM		$c(\frac{1}{2})$/W		FWHM(Hβ_{BC})		R_{FeII}		Γ_{soft}	
	r_S	P_{r_S}	r_S	P_{r_S}	r_S	P_{r_S}	r_S	P_{r_S}	r_S	P_{r_S}	r_S	P_{r_S}
	(1)	(2)	(3)	(4)	(5)	(6)	(7)	(6)	(9)	(10)	(11)	(12)
All Sources[b]												
$c(\frac{1}{2})$	0.411	5.951E-07	0.008	4.6E-01	0.970	8.7E-81	0.331	6.0E-05	-0.431	1.5E-07	-0.327	1.5E-04
W	···	···	0.141	5.5E-02	0.485	2.5E-09	0.469	9.1E-09	-0.530	4.5E-11	-0.284	9.1E-04
FWHM	···	···	···	···	0.040	3.3E-01	0.512	2.4E-10	-0.175	2.3E-02	-0.354	4.2E-05
$c(\frac{1}{2})$/W	···	···	···	···	···	···	0.381	3.9E-06	-0.471	7.8E-09	-0.336	9.9E-05
RQ [c]												
$c(\frac{1}{2})$	0.634	1.467E-09	-0.206	4.2E-02	0.959	8.2E-40	0.365	8.7E-04	-0.498	5.0E-06	-0.396	7.2E-04
W	···	···	-0.008	4.7E-01	0.783	3.6E-16	0.488	7.9E-06	-0.529	1.1E-06	-0.424	3.0E-04
FWHM	···	···	···	···	-0.206	4.2E-02	0.392	3.6E-04	0.056	3.2E-01	-0.296	9.7E-03
$c(\frac{1}{2})$/W	···	···	···	···	···	···	0.393	3.5E-04	-0.538	6.5E-07	-0.401	6.2E-04
RL[d]												
$c(\frac{1}{2})$	-0.024	4.3E-01	-0.108	2.1E-01	0.965	4.0E-35	-0.068	3.0E-01	-0.107	2.1E-01	-0.048	3.6E-01
W	···	···	0.145	1.4E-01	-0.095	2.4E-01	0.219	4.8E-02	-0.371	1.9E-03	-0.004	4.9E-01
FWHM	···	···	···	···	-0.092	2.4E-01	0.482	5.5E-05	-0.225	4.3E-02	-0.137	1.5E-01
$c(\frac{1}{2})$/W	···	···	···	···	···	···	-0.049	3.6E-01	-0.083	2.7E-01	0.001	5.0E-01
Pop. A[e]												
$c(\frac{1}{2})$	0.668	3.1E-08	-0.384	2.5E-03	0.978	5.3E-36	0.257	3.3E-02	-0.549	1.3E-05	-0.504	1.8E-04
W	···	···	-0.299	1.6E-02	0.746	1.1E-10	0.127	1.8E-01	-0.555	9.8E-06	-0.364	6.4E-03
FWHM	···	···	···	···	-0.279	2.3E-02	0.327	9.0E-03	0.113	2.1E-01	-0.281	2.9E-02
$c(\frac{1}{2})$/W	···	···	···	···	···	···	0.250	3.7E-02	-0.542	1.7E-05	-0.484	3.3E-04
Pop. B[f]												
$c(\frac{1}{2})$	0.032	3.905E-01	-0.067	2.8E-01	0.967	3.5E-47	-0.015	4.5E-01	-0.167	7.2E-02	-0.118	1.6E-01
W	···	···	0.089	2.2E-01	0.080	2.4E-01	0.092	2.1E-01	-0.134	1.2E-01	-0.006	4.8E-01
FWHM	···	···	···	···	-0.060	3.0E-01	0.481	4.1E-06	-0.068	2.8E-01	-0.260	1.4E-02
$c(\frac{1}{2})$/FWHM	···	···	···	···	···	···	-0.005	4.8E-01	-0.184	5.3E-02	-0.080	2.5E-01

[a]The number P in parenthesis yields the probability that the coupled variables are not correlated. A significant correlation can be assumed if $P \lesssim 0.01$.

[b]130 sources of which 118 with available Γ_{soft}.

[c]71 sources of which 62 with available Γ_{soft}.

[d]59 sources of which 56 with available Γ_{soft}.

[e]52 sources of which 46 with available Γ_{soft}.

[f] 78 sources, of which 72 with available $\Gamma_{\rm soft}$.

Table 5. Main Trends Along the 4DE1 Sequence

Parameter	Population A	Population B	References
FWHM(H$\beta_{\rm BC}$)	800 – 4000 km s^{-1}	4000 – 10000 km s^{-1}	1,2,3,4,5
•log $M_{\rm BH}$	6.5 – 8.5	8.0 – 10.0	6,7,8,9
• $L_{\rm bol}/L_{\rm Edd}$	0.1 – 1.0	0.01 – 0.5	6,7,8,9
W(H$\beta_{\rm BC}$)	$\sim$ 80 Å	$\sim$ 100 Å	1,2,3,4
H$\beta_{\rm BC}$ profile shape	Lorentzian	double Gaussian	2,3,5,10,11
$c(\frac{1}{2})$ H$\beta_{\rm BC}$	$\sim$ zero	+500 km s^{-1}	1,2,3
$R_{\rm FeII}$	0.7	0.3	1,2
SiIII] / CIII]	0.4	0.2	12,13
• log $n_{\rm e}$	11	9.5 – 10	12
• log U	–2/–1.5	–1.0/–0.5	12
FWHMCIVλ1549$_{\rm BC}$	(2–6) $\cdot 10^3$ km s^{-1}	(2–10) $\cdot 10^3$ km s^{-1}	this paper
W(CIVλ1549$_{\rm BC}$)	58 Å	105 Å	this paper
AI(CIVλ1549$_{\rm BC}$)	–0.1	0.05	this paper
$c(\frac{1}{2})$CIVλ1549	–800 km s^{-1}	zero	2,3,this paper,14,15
$\Gamma_{\rm soft}$	often large	rarely large	2,3,16
X-ray variability	extreme/rapid common	less common	17,18
optical variability	possible	more frequent/higher amplitude	19
probability radio loud	$\approx$ 3–4%	$\approx$ 0.25 %	2,20,21
BALs	extreme BALs	less extreme BALs	22,23

References. — 1: Marziani et al. (1996) 2: Sulentic et al. (2000a) 3: Sulentic et al. (2000b) 4: Marziani et al. (2003a) 5: Véron-Cetty et al. (2001) 6: Kaspi et al. (2000) 7: Marziani et al. (2003b) 8: Peterson et al. (2004) 9: Sulentic et al. (2006a); 10: Sulentic et al. (2002) 11: Sulentic et al. (2000c) 12: Marziani et al. (2001) 13: Wills et al. (1999) 14: Yuan & Wills (2003) 15: Baskin & Laor (2005) 16: Wang et al. (1996) 17: Turner et al. (1999) 18: Grupe et al. (2001) 19: Giveon et al. (1999) 20: Sulentic et al. (2003) 21: Sulentic et al. (2007), in preparation 22: Reichard et al. (2003) 22: Sulentic et al. (2006b)

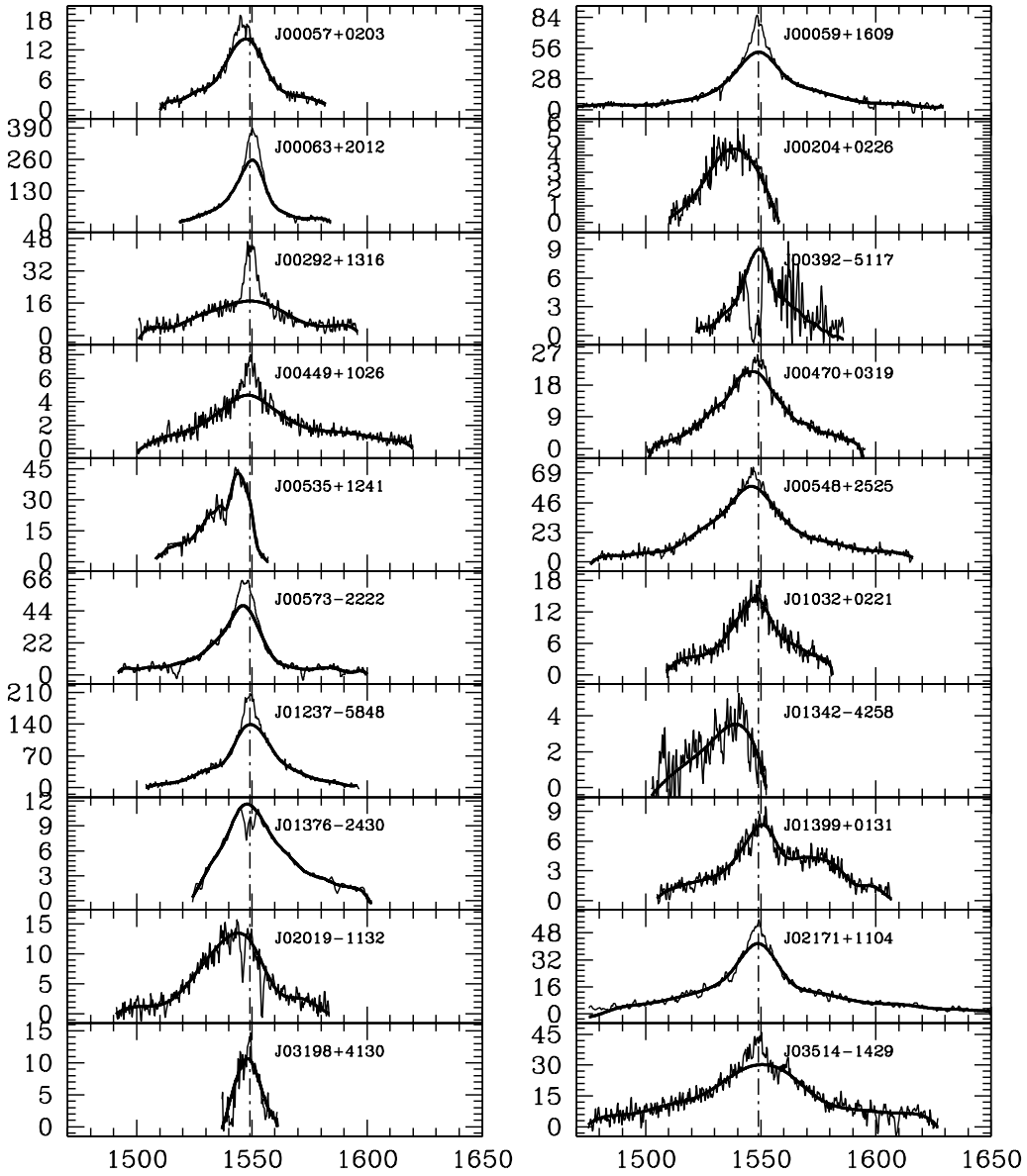

Fig. 1.— CIVλ1549 profiles for the 130 AGN used in the present study. They are presented in right ascension order. Abscissa is rest-frame wavelength (Å); ordinate is rest-frame specific flux (10^{-15} ergs s^{-1}cm^{-2} Å^{-1}). Thick curves are a high-order spline fits to CIVλ1549$_{\rm BC}$ and anything above it is considered to be narrow line emission. The major thick spacing (50 Å) corresponds to a radial velocity range of $\Delta v_{\rm r} \approx$ 9700 km s^{-1}.

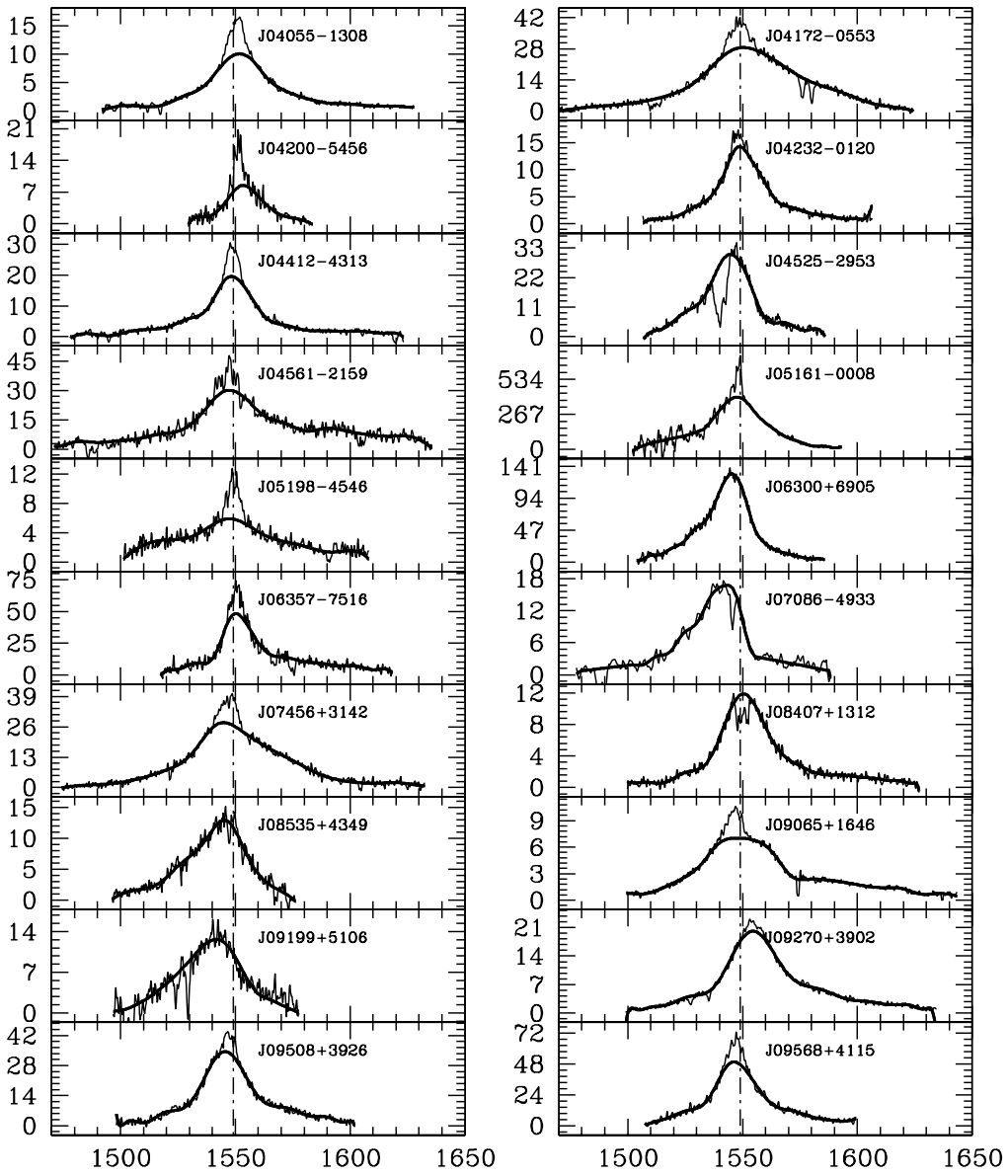
J04055−1308
J04200−5456
J04412−4313
J04561−2159
J05198−4546
J06357−7516
J07456+3142
J08535+4349
J09199+5106
J09508+3926
J04172−0553
J04232−0120
J04525−2953
J05161−0008
J06300+6905
J07086−4933
J08407+1312
J09065+1646
J09270+3902
J09568+4115
1500
1550
1600
1650

Fig. 1.— Cont.

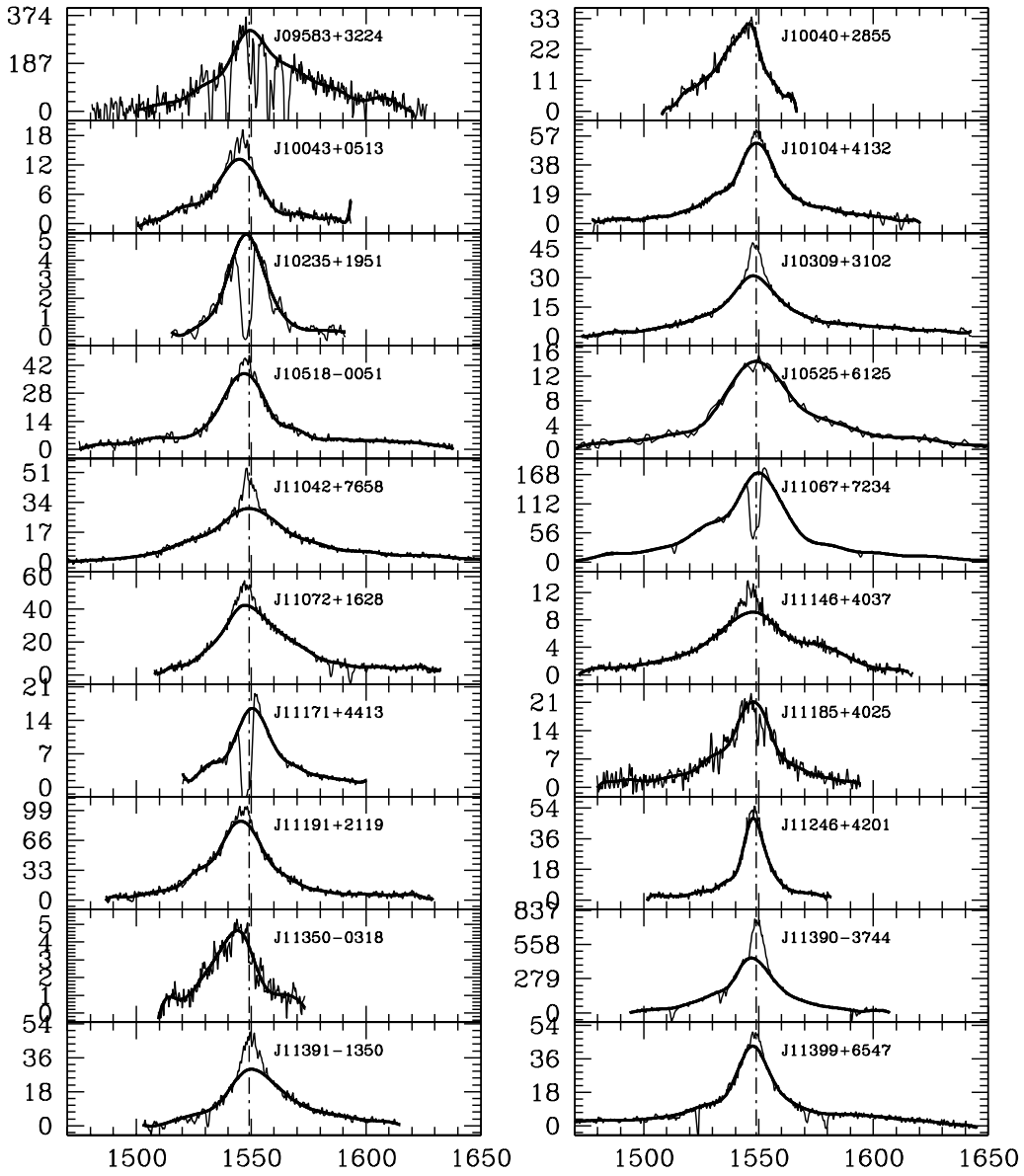
J09583+3224
J10040+2855
J10043+0513
J10104+4132
J10235+1951
J10309+3102
J10518−0051
J10525+6125
J11042+7658
J11067+7234
J11072+1628
J11146+4037
J11171+4413
J11185+4025
J11191+2119
J11246+4201
J11350−0318
J11390−3744
J11391−1350
J11399+6547
1500
1550
1600
1650

Fig. 1.— Cont.

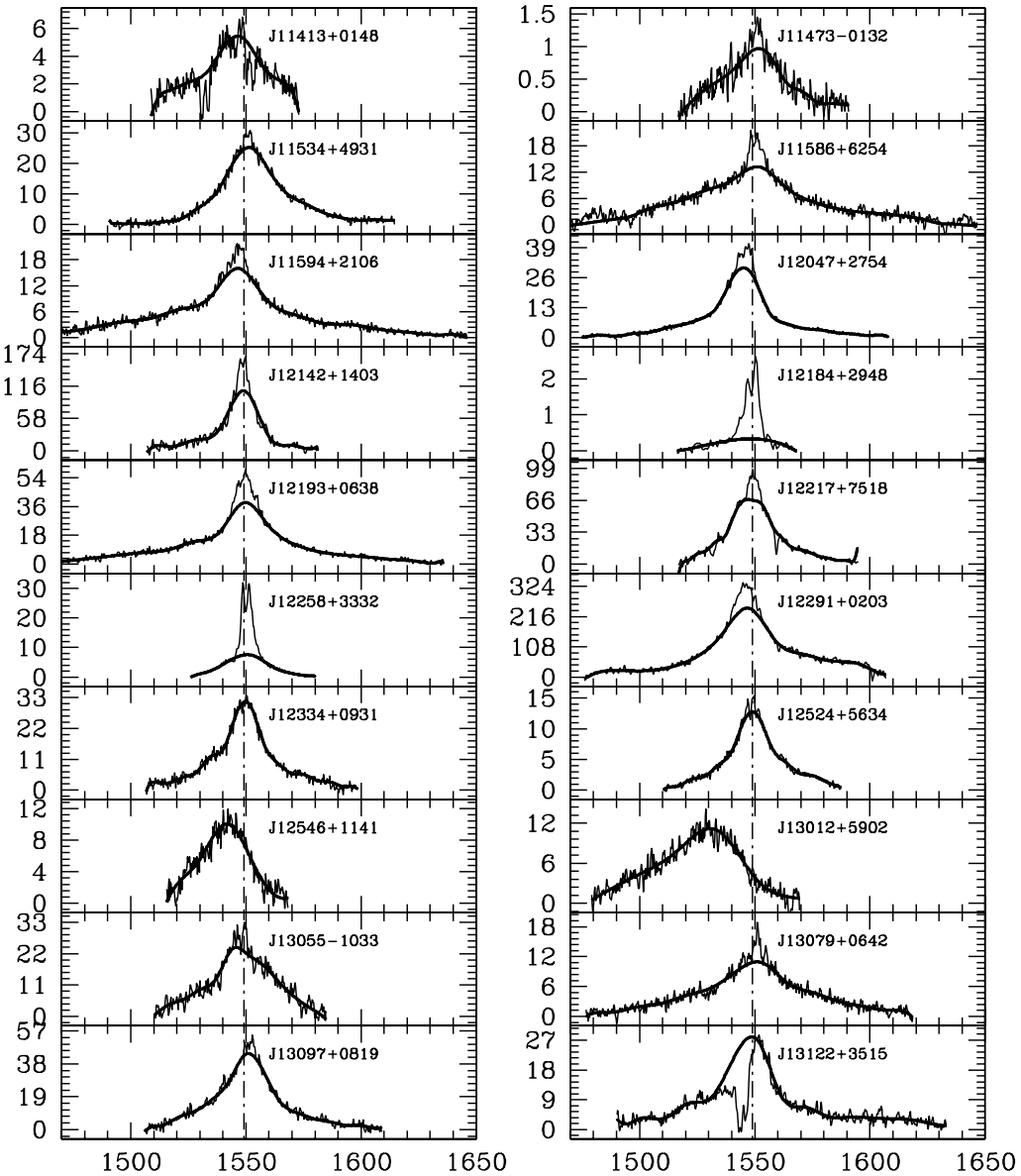
J11413+0148
J11473−0132
J11534+4931
J11586+6254
J11594+2106
J12047+2754
J12142+1403
J12184+2948
J12193+0638
J12217+7518
J12258+3332
J12291+0203
J12334+0931
J12524+5634
J12546+1141
J13012+5902
J13055−1033
J13079+0642
J13097+0819
J13122+3515
1500
1550
1600
1650

Fig. 1.— Cont.

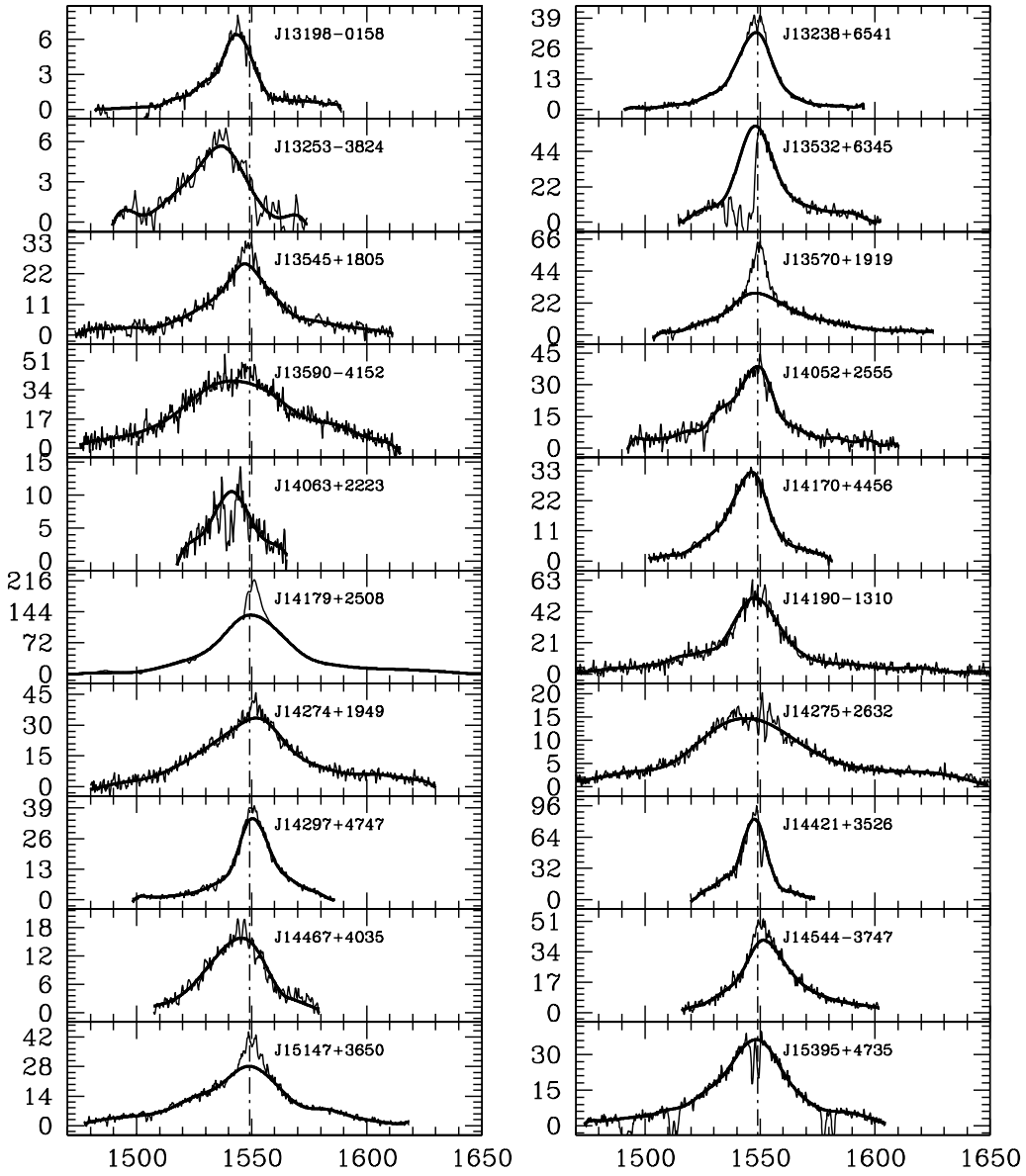
J13198−0158
J13253−3824
J13545+1805
J13590−4152
J14063+2223
J14179+2508
J14274+1949
J14297+4747
J14467+4035
J15147+3650
J13238+6541
J13532+6345
J13570+1919
J14052+2555
J14170+4456
J14190−1310
J14275+2632
J14421+3526
J14544−3747
J15395+4735
1500
1550
1600
1650

Fig. 1.— Cont.

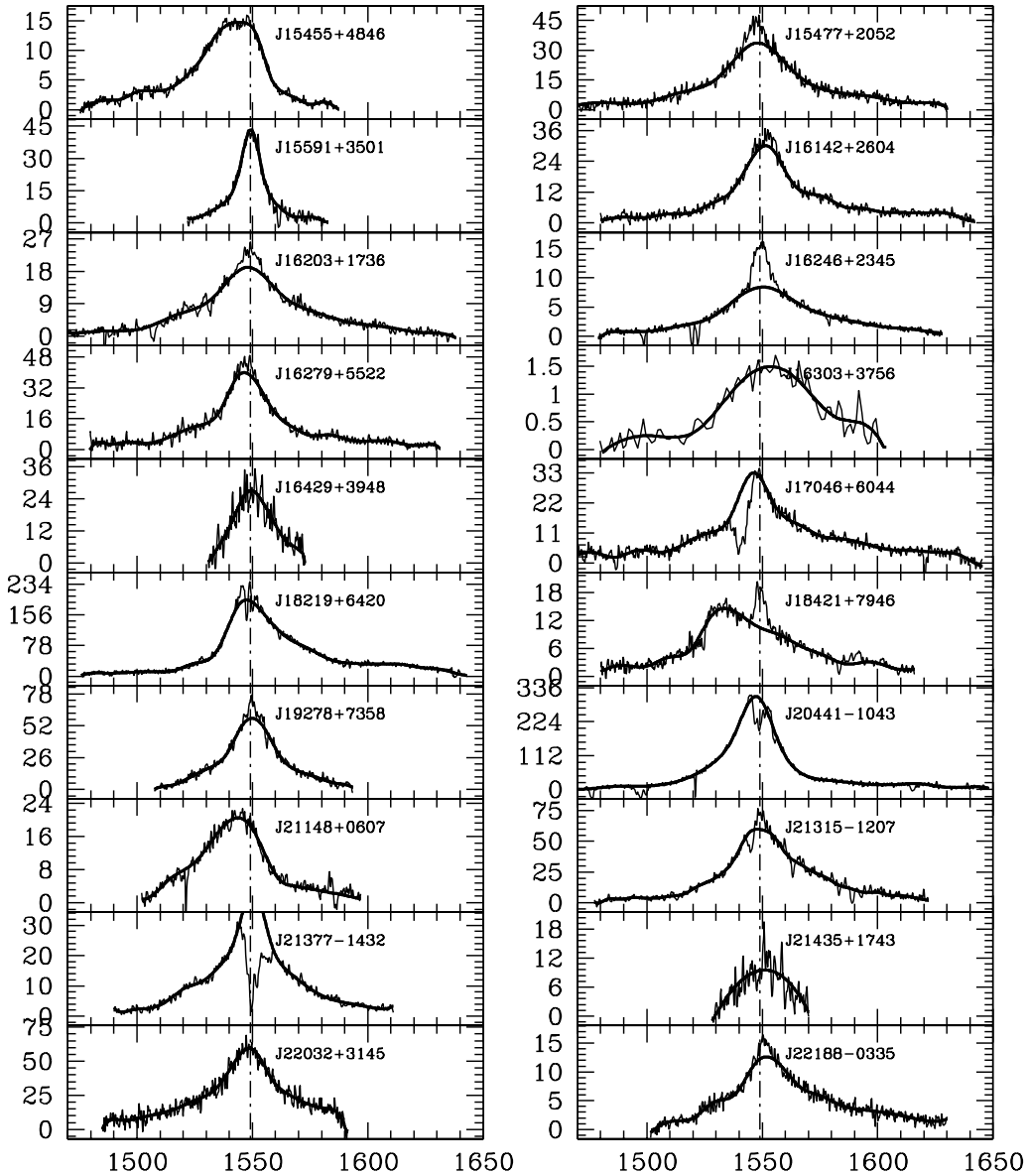
J15455+4846
J15591+3501
J16203+1736
J16279+5522
J16429+3948
J18219+6420
J19278+7358
J21148+0607
J21377−1432
J22032+3145
J15477+2052
J16142+2604
J16246+2345
J16303+3756
J17046+6044
J18421+7946
J20441−1043
J21315−1207
J21435+1743
J22188−0335
1500
1550
1600
1650

Fig. 1.— Cont.

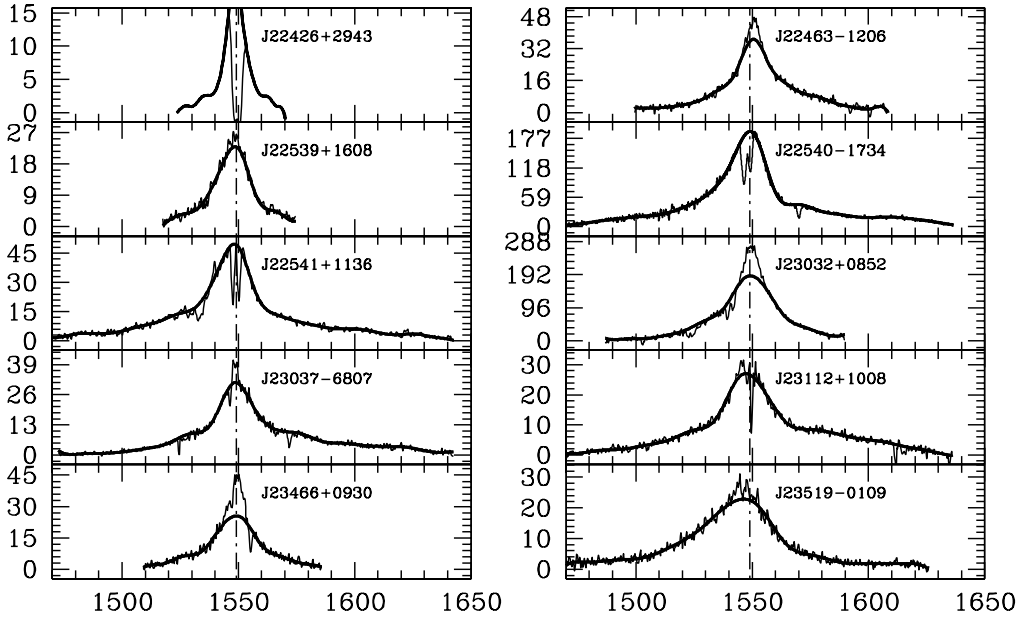
J22426+2943
J22539+1608
J22541+1136
J23037−6807
J23466+0930
J22463−1206
J22540−1734
J23032+0852
J23112+1008
J23519−0109
1500
1550
1600
1650

Fig. 1.— Cont.

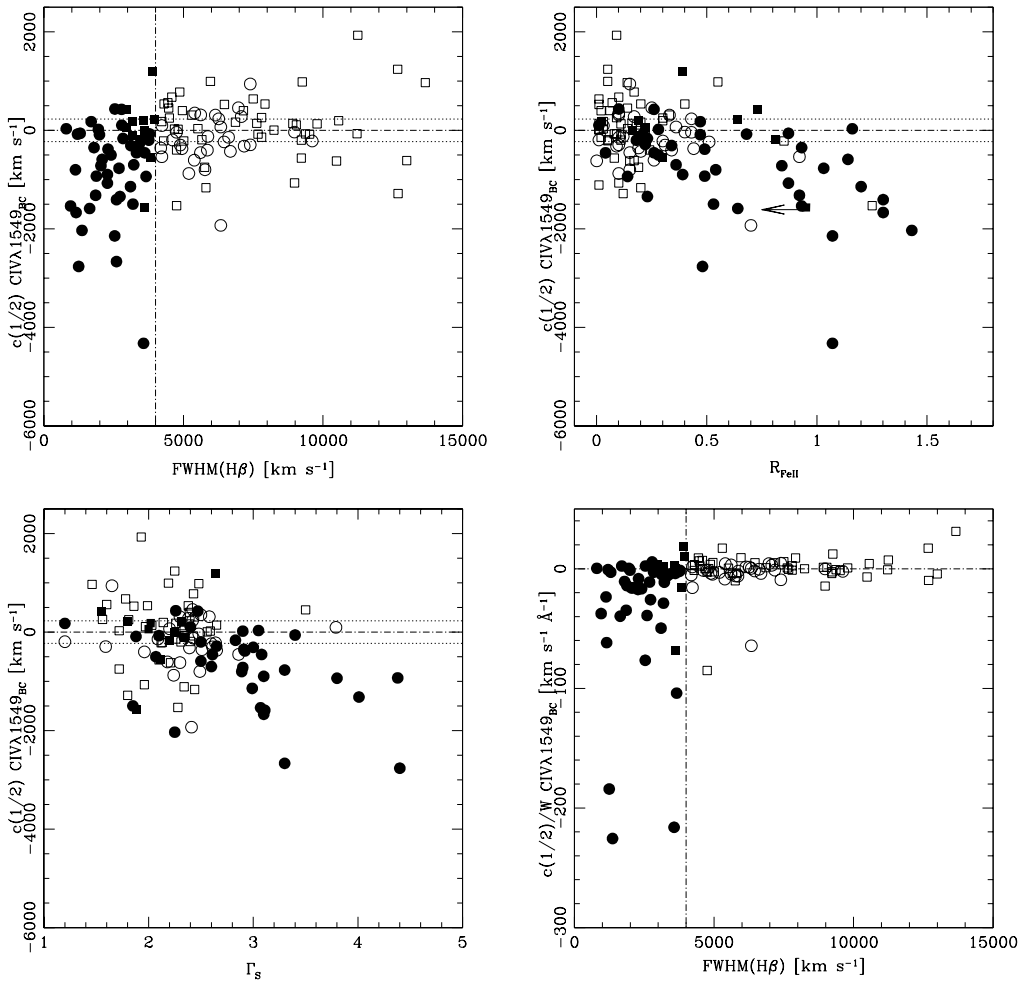

Fig. 2.— 4DE1 parameter planes involving C IVλ1549$_{\rm BC}$ profile shift at half-maximum ($c(\frac{1}{2})$, see text) vs. FWHM(H$\beta_{\rm BC}$) (in km s^{-1}) (UL), $R_{\rm FeII}$ (UR) and $\Gamma_{\rm soft}$ (LL). In LR we also show $c(\frac{1}{2})$ normalized by EW C IVλ1549$_{\rm BC}$ in order to emphasize the difference between Pop. A and B sources which are denoted with filled and open symbols respectively; radio-loud sources are represented by squares and radio-quiet by circles. The vertical line in the UL and LR panels marks the nominal Pop. A-B boundary. Dotted lines indicate $\pm$ 2 σ confidence intervals for $c(\frac{1}{2})$ (see §2.2) meaning that sources within that range do not show significant C IVλ1549 line shift.

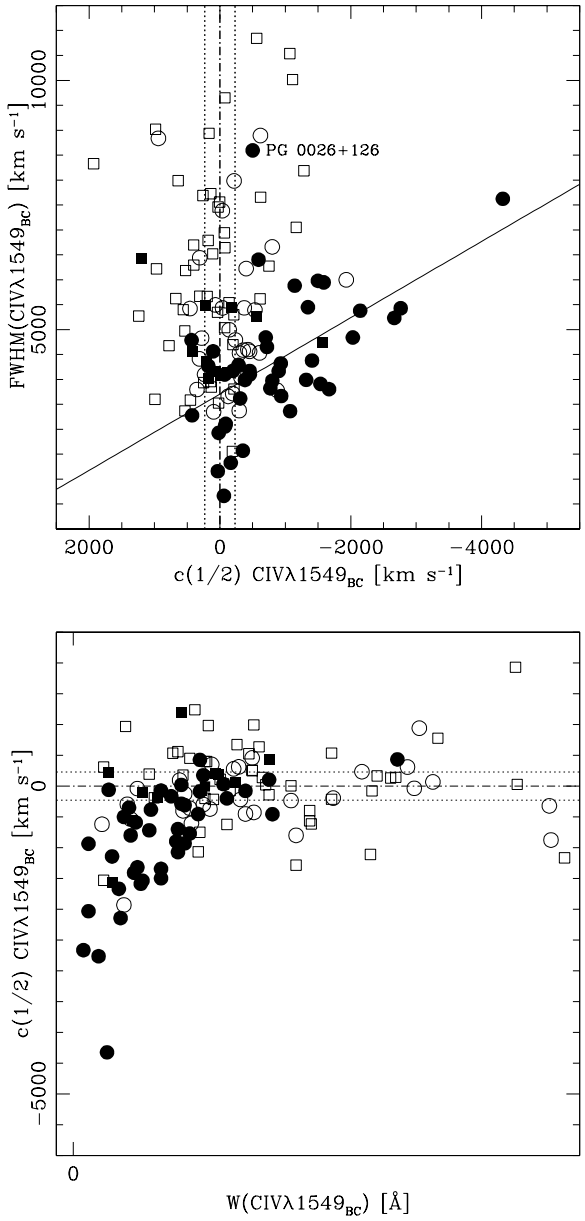

Fig. 3.— Upper panel: Correlation diagram for measures of FWHM CIVλ1549$_{\rm BC}$ vs. $c(\frac{1}{2})$ for Pop. B and Pop. A sources. Symbols and $c(\frac{1}{2})$ confidence intervals are same as in the previous Figure. The best fit regression line (lsq, unweighted) for the Pop. A correlation (RQ only) is shown. Both $c(\frac{1}{2})$ and FWHM(CIVλ1549$_{\rm BC}$) are in units of km s^{-1}. See Appendix A for a discussion of the outlier PG 0026+126. Lower panel: $c(\frac{1}{2})$ vs. rest-frame W(CIVλ1549$_{\rm BC}$).

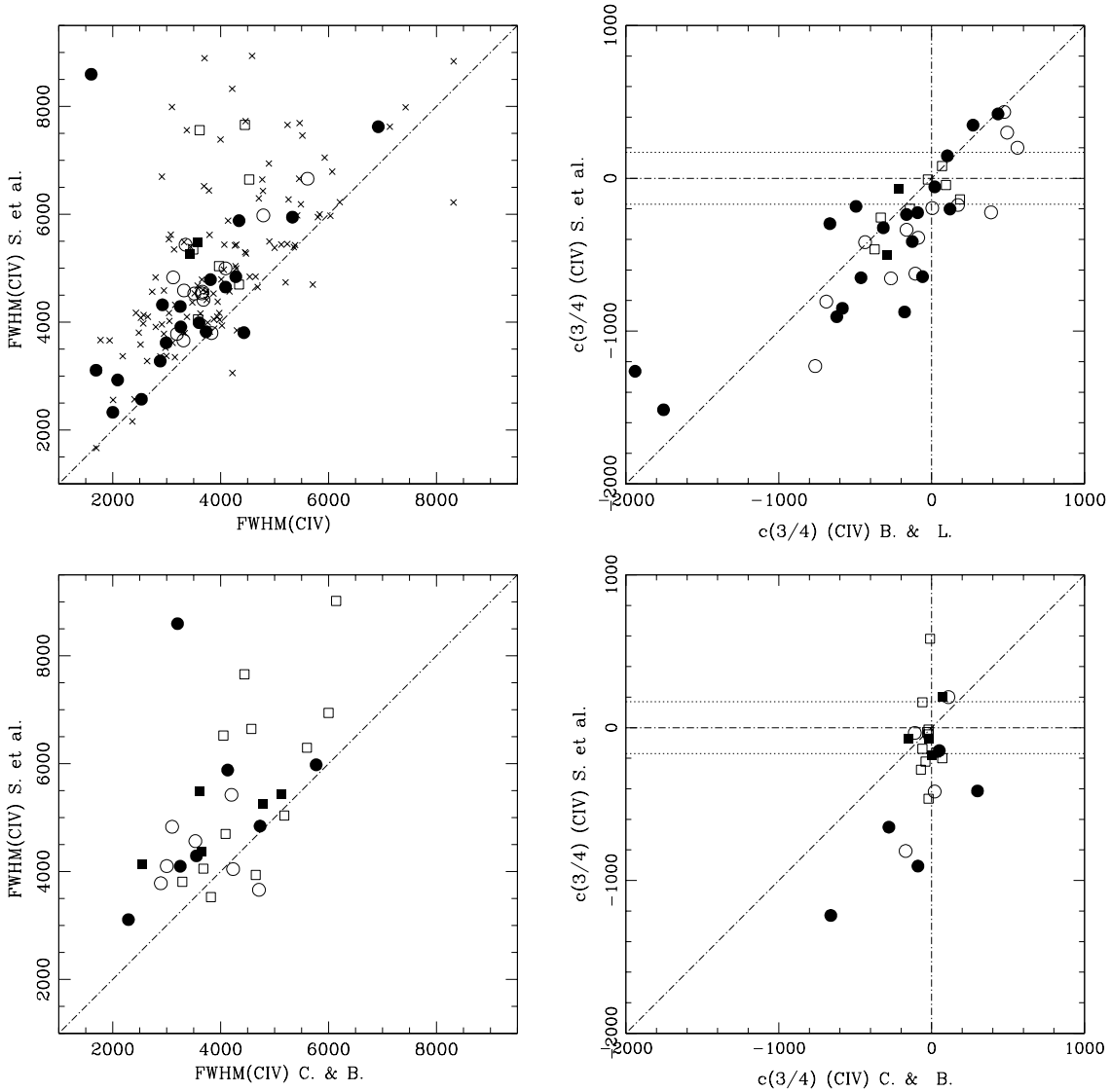

Fig. 4.— Comparison of our CIVλ1549$_{\rm BC}$ measures with those of Baskin & Laor (2005) and Warner et al. (2004) (upper panels) and Corbin & Boroson (1996) (lower panels). Left panels: FWHM(CIVλ1549$_{\rm BC}$) comparison, in units of km s^{-1}. Small crosses compare with FWHM(CIVλ1549) data of Warner et al. (2004). The same symbols used in previous figure were used for comparisons with Baskin & Laor (2005) and Corbin & Boroson (1996). Right panels: comparison CIVλ1549 line centroid at 3/4 intensity ($c(\frac{3}{4})$), in km s^{-1}. Our $c(\frac{3}{4})$ confidence intervals are shown in the right panels. The source with the largest blueshift (Pop. A quasar PG 1259+593) falls outside the boundary of the plot ($c(\frac{1}{2}) \approx 4000$ km s^{-1}). Data point for PG 0026+129 is not shown to avoid x-scale compression. Parity diagonal line is shown in all panels. Dotted lines indicate $\pm$ 2 σ confidence intervals for $c(\frac{3}{4})$ (see §2.2).

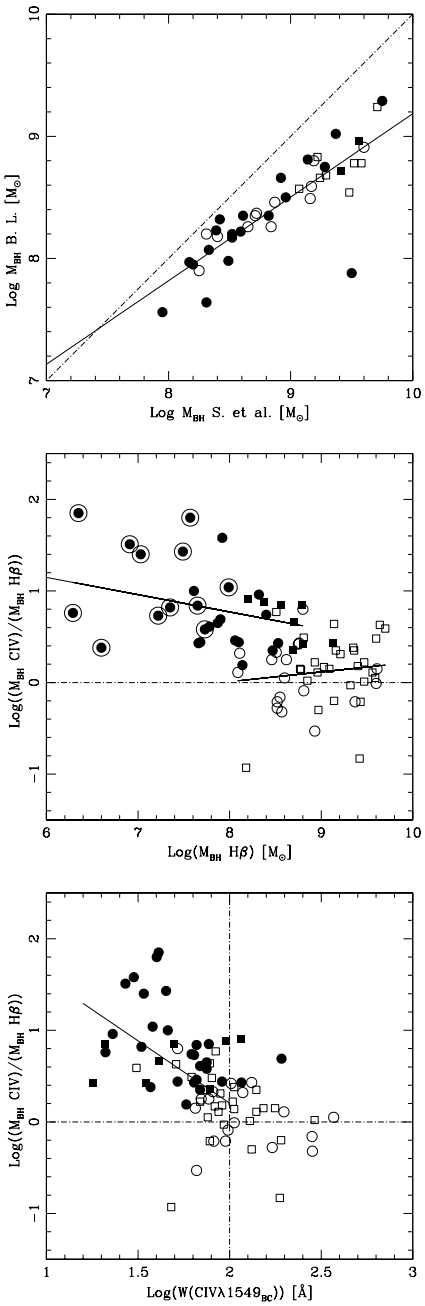

Fig. 5.— Upper panel: Comparison of our log $M_{\rm BH}$ estimates for sources in common with Baskin & Laor (2005). "Virial" velocity values derived from FWHM CIVλ1549$_{\rm BC}$ measures in both samples. Dot-dash indicates parity line. The thin line shows an unweighted lsq best fit for all sources. Middle panel: log ratio of $M_{\rm BH}$ estimated from CIVλ1549 and "corrected" H$\beta_{\rm BC}$ (see text in §5) vs. log $M_{\rm BH}$for sources in common with Marziani et al. (2003a). Thin lines show independent best fits (unweighted lsq) for Pop. A and B sources. NLSy1 sources are identified among Pop. A sources by a larger open circle. Lower panel: log ratio of $M_{\rm BH}$ estimated from CIVλ1549 and "corrected" Hβ as in panel above versus $\log W$(CIVλ1549$_{\rm BC}$). Thin line shows a best fit (unweighted lsq) for all sources with $\log W$(CIVλ1549$_{\rm BC}$)< 2.

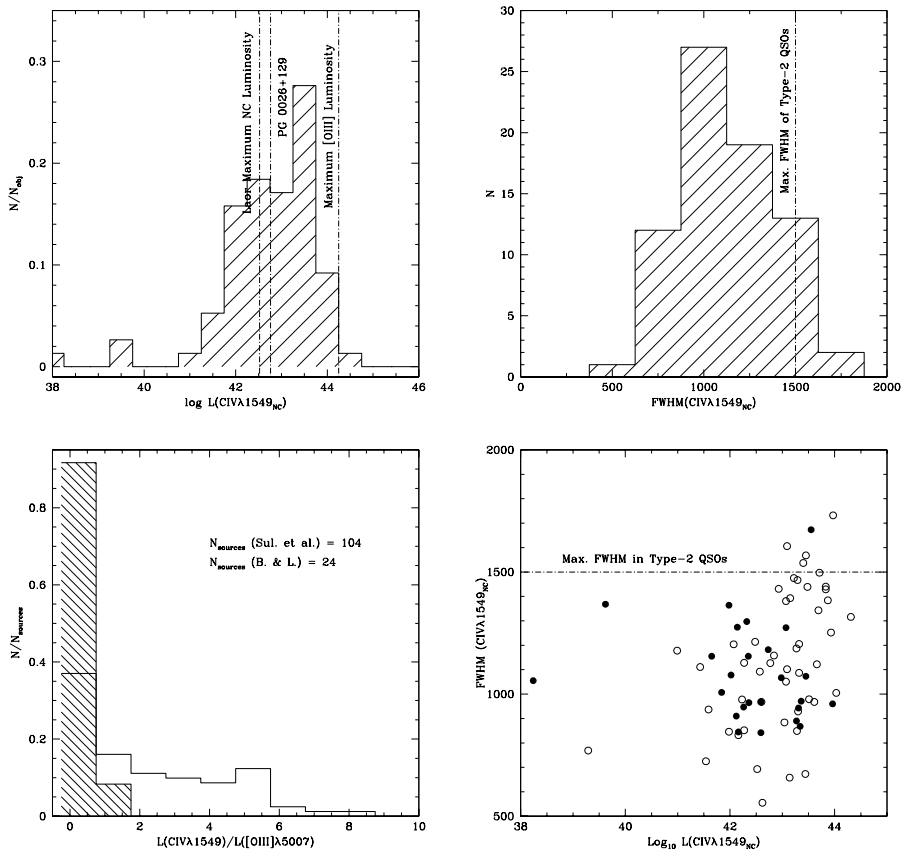

Fig. 6.— Civλ1549$_{\rm NC}$ analysis. UL: luminosity distribution of Civλ1549$_{\rm NC}$ components identified in our HST sample ($\log L$(Civλ1549$_{\rm NC}$) in units of ergs s^{-1}; shaded histogram); UR: FWHM distribution for Civλ1549$_{\rm NC}$ components; LR: distribution of the ratio L(Civλ1549$_{\rm NC}$)/L([Oiii]λ5007) for our HST sample (corrected for Galactic extinction) and for sample of Baskin & Laor (2005). LR: FWHM(Civλ1549$_{\rm NC}$) vs. $\log L$(Civλ1549$_{\rm NC}$) for our HST sample. Filled circles indicate Pop. A, open circles Pop. B sources.